Nano Energy (2015) 11, 436–462

Available online at www.sciencedirect.com

ScienceDirect

journal homepage: www.elsevier.com/locate/nanoenergy

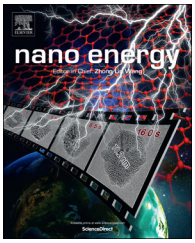

REVIEW

Triboelectric nanogenerators as self-powered active sensors

Sihong Wang[a,1], Long Lin[a,1], Zhong Lin Wang[a,b,*]

[a]School of Materials Science and Engineering, Georgia Institute of Technology, Atlanta, GA 30332-0245, United States
[b]Beijing Institute of Nanoenergy and Nanosystems, Chinese Academy of Sciences, Beijing 100083, China

Received 5 October 2014; accepted 30 October 2014
Available online 8 November 2014

KEYWORDS
Triboelectric nanogenerators;
Contact electrification;
Mechanical energy harvesting;
Wireless sensor networks;
Self-powered systems;
Self-powered active sensors

Abstract
The development of internet of things and the related sensor technology have been a key driving force for the rapid development of industry and information technology. The requirement of wireless, sustainable and independent operation is becoming increasingly important for sensor networks that currently could include thousands even to millions of sensor nodes with different functionalities. For these purposes, developing technologies of self-powered sensors that can utilize the ambient environmental energy to drive the operation themselves is highly desirable and mandatory. The realization of self-powered sensors generally has two approaches: the first approach is to develop environmental energy harvesting devices for driving the traditional sensors; the other is to develop a new category of sensors – self-powered active sensors – that can actively generate electrical signal itself as a response to a stimulation/triggering from the ambient environment. The recent invention and intensive development of triboelectric nanogenerators (TENGs) as a new technology for mechanical energy harvesting can be utilized as self-powered active mechanical sensors, because the parameters (magnitude, frequency, number of periods, etc.) of the generated electrical signal are directly determined by input mechanical behaviors. In this review paper, we first briefly introduce the fundamentals of TENGs, including the four basic working modes. Then, the most updated progress of developing TENGs as self-powered active sensors is reviewed. TENGs with different working modes and rationally designed structures have been developed as self-powered active sensors for a variety of mechanical motions, including pressure change, physical touching, vibrations, acoustic waves, linear displacement, rotation, tracking of moving objects, and acceleration detection. Through combining the open-circuit voltage and the short-circuit current, the detection of both static and dynamic processes has been enabled. The integration of individual sensor elements into arrays or matrixes helps to realize the mapping or parallel detection for

*Corresponding author.
E-mail address: zlwang@gatech.edu (Z.L. Wang).
[1]These authors contributed equally.

http://dx.doi.org/10.1016/j.nanoen.2014.10.034

multiple points. On the other hand, the relationship between the amplitude of TENG-generated electrical signal and the chemical state of its triboelectric surface enables TENGs to function as self-powered active chemical sensors. Through continuous research on the TENG-based self-powered active sensors in the coming years to further improve the sensitivity and realize the self-powered operation for the entire sensor node systems, they will soon have broad applications in touch screens, electronic skins, healthcare, environmental/infrastructure monitoring, national security, and more.

Contents

Introduction

Self-powered sensing

Information technology is a major driving force for the modern world's development in the past decades. The collection and exchange of information rely on various types of sensors with different functionalities. The construction of large-scale sensor networks and systems can help to realize "internet of things", which correlate objects and devices to large databases and networks (the internet). By replacing the traditional finite number of discrete sensors with a large number of independent and mobile sensors distributed in the field, a statistical analysis of the signals collected through the internet can provide precise and reliable information, so that effective strategies can be taken in responding to the change in the environment. In a lot of cases, the sensor nodes are distributed across a wide range of area or embedded/implanted in closed locations, so that they need to operate wirelessly for important applications in implantable biosensors, patient monitoring, environmental and structure monitoring, and national security [1]. For these systems, it is very important for the sensor nodes to have the capability of operating independently, sustainably and maintenance-free. However, under the context of the current technology, most of sensors need power sources for driving their operations, which is a major limitation for realizing the aforementioned features for the wireless sensor networks. These power sources cannot be simply provided by batteries for two reasons: (i) the number of sensors to be involved in the sensor network will be huge and their locations could be difficult to track, so replacing individual batteries would represent a tremendous, even impossible task; and, (ii) the periodic replacement of batteries will create a huge amount of materials that are environmentally unfriendly and potentially hazardous to human health.

Therefore, realizing self-powered operation for the sensor nodes in the wireless sensor networks is critically

important for the broad applications of such networks, which is gradually becoming a major research direction in this area now and in the future [2,3]. The most feasible way to achieve self-powered operation is to harvest energy from ambient environment to drive a sensor node itself [4]. The energy harvesting device can directly serve as a sustainable power source for the sensor node or at least use together with a battery to replenish its energy consumption. Besides, if the sensor can generate electric signal itself as a response to the trigger or change in the environment, it can operate without an external power source, which is named as "active sensors". With this strategy, the sensor systems can be simplified and the total energy consumption can be largely reduced. Thus, developing self-powered active sensors can largely facilitate the wide range of application for wireless sensor networks.

Starting from 2006, our group has been developing a new technology – nanogenerators – for converting mechanical energies in different scales into electricity [5,6]. Besides the outstanding capability of serving as a sustainable power source for electronic devices, the produced electric signals from nanogenerators can also be utilized for directly sensing the applied mechanical actions without a power source. The first type of nanogenerators is based on the piezoelectric effect of semiconductor nanowires (e.g. ZnO, GaN) [5,7–10]. In the recent years, a new category of nanogenerators-triboelectric nanogenerators (TENGs) – has been invented and quickly developed on the basis of a universal effect – the contact electrification (also named as triboelectrification) [11–14], which has shown a large number of desirable advantages, such as extremely high output and efficiency, low cost, excellent versatility in structural design, outstanding stability and robustness, as well as environmental friendly [15–27]. Since the TENGs can generate electricity from any type of mechanical motions in the natural environment including touching [28,29], impact [30,31], linear sliding [32,33], rotation [21,34], vibration [35,36], and so on, they can serve as the self-powered active sensors for all these different types of mechanical motions. Besides, since the amplitude of the electrical signals generated by the TENGs are proportional to the surface triboelectric charge density that is determined by the chemical state of the surface, the TENGs can also be utilized as self-powered active chemical sensors [37,38].

Fundamentals and four basic modes of triboelectric nanogenerators

Triboelectric nanogenerators are based on the coupling of two effects: contact electrification and the electrostatic induction. The contact electrification is a universally-existing phenomenon in the nature and people's living life, and has been known for thousands of years. It describes a phenomenon that a material/surface becomes electrically charged after it gets into contact with a different material/surface [11–14,39]. The generated triboelectric charges on a dielectric surface can be preserved for a long time, which thus serve as the induction source for the electricity generation process in TENGs. Under the driving of external mechanical motions, the relative position of the triboelectrically-charged surface will change periodically in a TENG device, which will lead to the periodic variation of the induced potential difference between the two electrodes. In order to keep the electrostatic equilibrium between the two electrodes, the free electrons in the electrodes will be driven to flow back and forth to screen the induced potential difference. In this way, the applied mechanical energy is converted into electricity. With different configurations of the electrodes and/or different moving manners of the triboelectric layers to realize the electrostatic induction process, four fundamental modes of TENGs have been established (Fig. 1, from Ref. [40]), as elaborated in follows.

Vertical contact-separation mode

The vertical contact-separation mode [18,19,31] is the first fundamental mode of TENG with the simplest design as an example (Fig. 1a). In this mode, two films with distinctively-differed triboelectric polarities face with each other in a stacked configuration, at least one of which needs to be dielectrics. For dielectric film, electrode is attached on its outer surface, while a conductive triboelectric layer can serve as an electrode itself. Under a pressing force from an external motion, the two triboelectric layers can get into physical contact with each other, which generates oppositely charged surfaces. Subsequently, upon releasing, the two surfaces are separated by a small gap in the vertical-to-plane direction, which creates a potential drop across the two electrodes to drive the flow of electrons through the connected load. Once the gap is closed, the triboelectric-charge-created potential disappears, and the electrons will flow back to achieve electrical equilibrium.

In this mode, the electricity generation process requires the effective switching between the intimate contact state and the fully separated state. In order to achieve this, several different innovative device structures have been developed, such as the arch-shaped structure [19], the spring-supported structure [31] and so on. The TENGs based on this operation mode is very effective in harnessing short-range cyclic motions, e.g. vibrations and periodic impacts [35,36,41–44]. Besides, this mode provides several unique advantages for the practical applications of TENGs, such as high instantaneous power density, simple structure designs, and so on.

Lateral sliding mode

The lateral sliding mode has the same prototype device structure with the vertical contact-separation mode (Fig. 1b). The electricity is also generated through the periodic contact and separation between the two triboelectric surfaces [20,32]. Starting from the same contact state, the separation takes place in the in-plane direction through sliding the layers apart. This relative sliding between the two surfaces not only creates triboelectric charges on the two surfaces, but also produces a lateral polarization along the sliding direction. The induced potential will drive the electrons on the top and bottom electrodes to flow in order to fully balance the field created by the triboelectric charges. From the back-and-forth sliding cycles, an AC output is generated.

Such sliding processes can be obtained from planar motions [32,33], disc rotation [21], or cylindrical rotation [45].

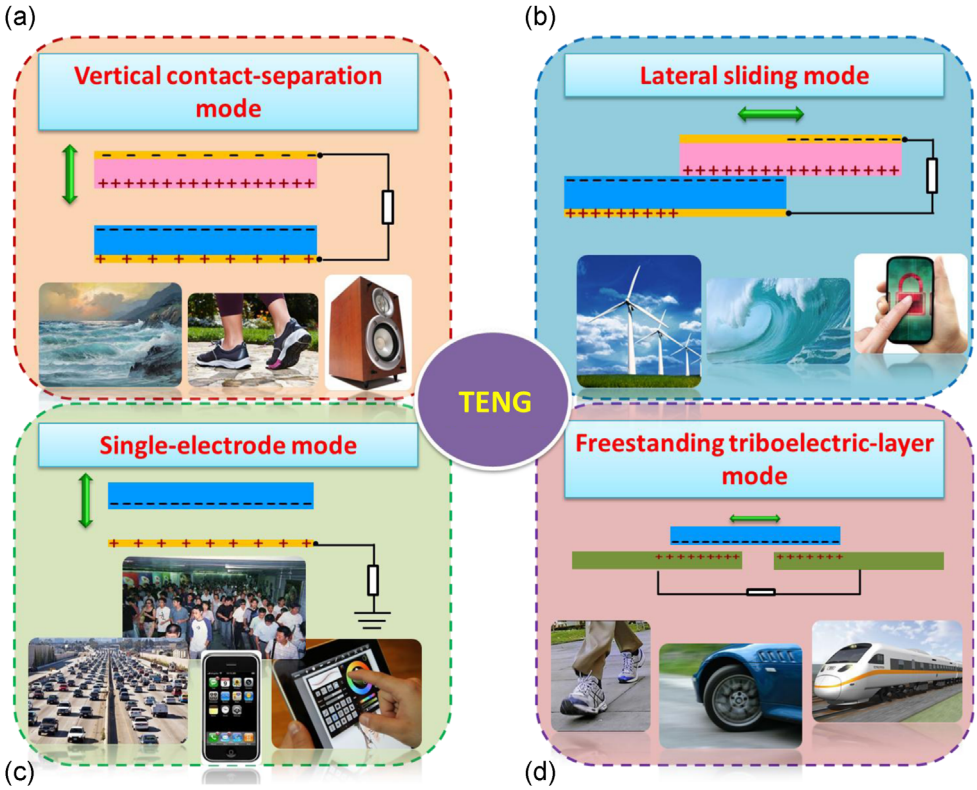

Fig. 1 Four fundamental modes of triboelectric nanogenerators: (a) vertical contact-separation mode; (b) lateral-sliding mode; (c) single-electrode mode; and (d) freestanding triboelectric-layer mode. Reproduced with permission from Royal Society of Chemistry [40].

Compared to the vertical contact-separation mode, this lateral sliding mode offers several important advantages. The generation of the triboelectric charges from the relative sliding between two surfaces is more effective than the pure contact. More importantly, through making the grated structures [20,33] for the sliding-mode TENGs, the in-plane charge separation-contact process can be enabled multiple times in a full sliding motion, which achieves more efficient charge transfer, thus significantly elevated power output.

Single-electrode mode

The two modes introduced above have two electrodes attached onto the moving triboelectric layers. In nature, a moving object is often naturally charged due to its contact with air or other object, such as the soles of our shoes and the human body. Thus, these moving objects can directly serve as the triboelectric layer in the TENG to induce the electricity generation process. However, in these cases if an electrode is required to be attached, it is very inconvenient for the practical applications. In this regard, we introduced a single electrode TENG [26,46], in which only one electrode directly interact with the moving triboelectric layer. The other electrode is just a reference electrode as a source for electron, which can be a large conductor or just the ground (Fig. 1c). If the size of the TENG is finite, an approaching or departing of the top object from the electrode would change the local electrical field distribution, so that there are electron exchanges between the bottom electrode and the reference electrode or the ground to keep the balanced potential between them.

In this mode, although the electrostatic induced electron transfer between the two electrodes is not the best in effectiveness due to the electrostatic screening effect [47], the charged object can have a free moving without any restriction. The relative movement between the triboelectric layer and the electrode can be both vertical contact-mode [26] and lateral sliding-mode [46], and even the hybridization of the two modes [48]. This advantage makes the single-electrode-mode TENG particularly suitable for acting as a self-powered active sensor to detect any electrically-charged object.

Freestanding triboelectric-layer mode

When harvesting energy from a free-moving triboelectrically-charged object, the two stationary electrodes can have a symmetric configuration in TENG device. The movement of a freestanding triboelectric layer brings it to alternatively approach either one of the two electrodes, so that the induced potential difference will be periodically reversed. An AC output will be driven to flow through the external load. This is the freestanding-triboelectric-layer mode of TENG [22]. Compared to the above single electrode mode, there is no screening effect in this mode, so that the electrostatically-induced electron transfer can be most effective to reach the same amount of triboelectric charges on the freestanding layer. Thus, when serving as an energy harvesting, this mode is much more efficient than the single-electrode mode.

The freestanding triboelectric-layer mode can have two typical configurations. In the first type, the two stationary

sits on the same plane, and the triboelectric layer slides between the overlapping positions of the two electrodes [22,34,49]. Compared to the sliding-mode introduced in the Lateral sliding mode section, the triboelectric layer doesn't need to maintain the contact with the electrode layer during the sliding. It means this mode enables non-contact sliding operation. This advantage largely improves the energy conversion efficiency as well as the long-term stability of the generator by avoiding the direct friction between the two surfaces. Moreover, due to the capability of non-contact operation, this pair of electrodes can be laminated underneath a dielectric film. In the second type of basic structure, the two electrodes are configured face-to-face and the freestanding triboelectric layer oscillates up-and-down in the gap between the electrodes to enable a vertical contact-separation mode [50]. Because of the constant capacitance between the electrodes and the confined electric field, the electricity generation behavior has a linear characteristic, which not only enables non-contact operation for the vertical contact mode with the above described advantages as well, but also can serve as the basis for quantitative sensing. Using such a design, we have demonstrated the harvesting of energy from human walking and a moving automobile, showing the potential for harvesting energy from a freely moving object without an electric connection.

Triboelectric nanogenerators as self-powered active pressure/touch sensors

Based on the above-mentioned working principle of the TENGs, the output performance (open-circuit voltage, short-circuit current, etc.) of a TENG is largely affected by magnitude/frequency of the external mechanical stimuli, among which the normal pressing is one of the most common types. In this regard, the most straightforward application for TENG-based active sensors would be the monitoring of external pressure/touch applied onto the TENG [17,28-30]. It has been demonstrated that the open-circuit voltage can be utilized for static measurement of the magnitude of the applied pressure, while the short-circuit current is more suitable for dynamic measurement on the loading rate of the applied pressure [30]. Based on this basic principle, several prototypes have been developed that displayed high sensitivity, fast response, and low power consumptions. Moreover, the integrations of triboelectric pressure sensor array have been fulfilled for pressure imaging/mapping, and highly selective profile of the applied pressure was visualized through both electric measurement and the power up of light illuminations [25,29,30,51]. These demonstrations of pressure detection and tactile imaging will open up many potential applications in electronic skins, touch screens, security checking, health monitoring, and so on.

Self-powered pressure sensors based on vertical contact-separation mode TENGs

Among the four fundamental modes of TENGs, the vertical contact-separation mode is the most convenient way to demonstrate the pressure sensing capabilities. The first proof-of-concept demonstration was realized on a transparent flexible nanogenerator (FTNG) [17], with the micro-patterned plastic surface to enhance the triboelectric charge density. Such self-powered pressure sensor can sense gentle pressures like a water droplet (8 mg, ~3.6 Pa in contact pressure) and a falling feather (20 mg, ~0.4 Pa in contact pressure) through relative deformation between two polymer sheets by external mechanical forces.

To obtain a more quantitative understanding and characterization about the contact-mode TENG based active pressure sensor, a triboelectric active sensor (TEAS) was developed and comprehensively characterized to reveal its basic sensing capabilities [30]. As shown in Fig. 2a, the device structure of the TEAS consists of a PDMS membrane modified with micro-patterned pyramid structures (Fig. 2b), and a piece of aluminum thin film assembled with the composite of silver nanowires and nanoparticles (Fig. 2c). The micro/nano structures on both inner surfaces were introduced to enhance the triboelectric charge density on the two surfaces, which would help to improve the pressure response of the TEAS. By correlating the output behavior of the TEAS with the elastic property of polymer materials, the relationship between the open-circuit voltage and the applied pressure could be analyzed by the following equation:

$$\frac{V_{OC,0}-V_{OC}}{V_{OC,0}}=\frac{d_o-d}{d_0}=\frac{S}{k\times d_0}\times p \quad (1)$$

hence the relative variation of the V_{OC} should be expected to show direct linear relationship with the applied pressure, and thus it was a reliable parameter for measuring the magnitude of the external pressure applied onto the TEAS, while the J_{SC} was able to provide the dynamic information of the applied pressure (i.e. loading rate). Combining the analysis on the measurement of both the V_{OC} and the J_{SC}, the TEAS device was capable of giving the detailed information about the ambient mechanical stimulations. Fig. 2d is the real-time measurement result of V_{OC} under series of different pressures. The reference state of voltage was selected in the way that the V_{OC} approached 0 with the maximum pressure when the two surfaces came into full contact. It could be observed that the V_{OC} stays at the maximum level (V_0=60 V) when there is no pressure, and decreases to a lower level once the external pressure is applied. The relationship between relative voltage variation $(V_0-V)/V_0$ and magnitude of pressure was plotted in Fig. 2e. In the low pressure region (Region I), the sensitivity of the TEAS is 0.31 kPa^{-1}, which was much higher than that of the high pressure region (0.01 kPa^{-1} in Region II), since the gap distance was close to zero from the turning point in Region II, and the increasing pressure only worked for enhancing the effective contact area between the two layers. The separated fittings of the data in both regions displayed good linear behavior (R_I^2=0.965, and R_{II}^2=0.985), which revealed the validity of the device as a reliable pressure sensor. Further measurement results revealed that the voltage response was independent of the loading rate if the magnitude of pressure was kept constant, indicating the V_{OC} is a static signal for pressure measurement. On the other hand, the J_{SC} was not only dependent on the applied force/pressure, but also related to the loading rate of the external force. Furthermore, the output profile of the J_{SC}

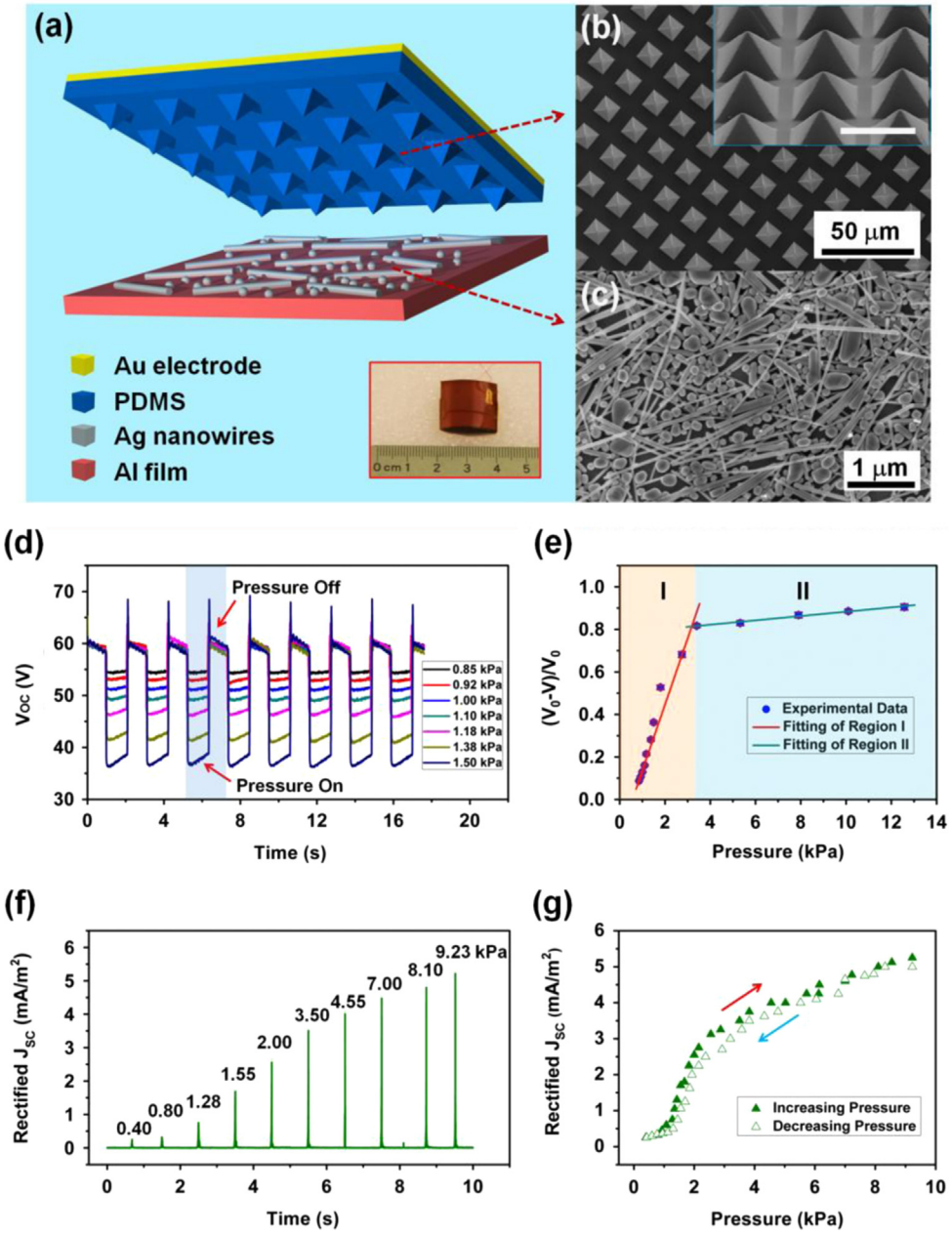

Fig. 2 Self-powered pressure sensor based on contact mode TENG. (a) Schematic structure of the triboelectric active sensor. Inset: a photograph of the triboelectric active sensor. (b) Top-view SEM image of the pyramid microstructure on the surface of the PDMS thin film. Inset: an enlarged 30°-tilted view SEM image of the microstructure. The scale bar is 10 μm. (c) The SEM image of the silver nanowire/nanoparticles assembly on the surface of the aluminum foil. (d) The real time measurement of the open-circuit voltage of the triboelectric active sensor upon different pressures. (e) The summarized relative change of the open-circuit voltage with different pressures. (f) The real time measurement of the rectified short-circuit current of the triboelectric active sensor upon different pressures. (g) The summarized reversible behavior of the rectified short-circuit current with variable pressures. Reproduced with permission from American Chemical Society [30].

was a pulse-like current peak, which enables its application for dynamic pressure detection, as shown in Fig. 2f and g. The measured rectified J_{SC} with variable pressures under the same loading rate were displayed in Fig. 2f, showing a clearly increasing trend with elevated pressures. The full data summarized in Fig. 2g showed the reversibility of the current response. The loading pressure was first increased from low pressure regime (<1 kPa) to a high pressure regime (~ 9 kPa), and then decreased to the original magnitude. The resulted current response in the decreasing-pressure curve did not exhibit much deviation in reference to the original curve, thus demonstrating the reliability of the current measurement. Furthermore, it was discovered that the J_{SC} was also affected by the acceleration of the linear motor, which implied that the J_{SC} could be used as a dynamic factor for quantification of the loading

rate of the applied pressure. Both the static and dynamic pressure detection showed high stability after even 30,000 cycles of loading and unloading process, and a low-end detection limit of ~2 Pa was successfully demonstrated.

Since the applied contact pressure can be induced from magnetic force, then the TENG coupled with a permanent magnet can be applied as a self-powered sensor for actively monitoring the magnitude variation of the external magnetic field [52]. The output voltage of the sensor was found to exponentially increase with increasing magnetic field. The detection sensitivities for the change and the changing rate of magnetic field are about 0.0363 ln(mV)/G and 0.0497 ln(mV)/(G/s), respectively. The response time and reset time of the sensor are about 0.13 s and 0.34 s, respectively.

Self-powered touch sensors based on single-electrode TENGs

The sensors for instantaneous detection of touch are of critical importance for the applications of touch screen, security monitoring, healthcare and so on. Because of the single-electrode TENGs' unique advantage that electrode deposition on the moving part doesn't need the attachment of electrode, they are especially suitable for the detection of touch from a foreign object. The first active tactile sensor based on this mode was demonstrated through taking advantage of the interactions between human skins and PDMS [29]. The constructed TENG based on periodic contact/separation between a human skin patch and a PDMS was utilized as self-powered touch sensor directly from the tactile motion of human skin of a finger, with a high sensitivity of 0.29 V/kPa, and a low reset time of 0.1 s.

The performance of such active touch sensor was further enhanced by fabricating a self-powered triboelectric sensor on flexible thin film materials [28]. The schematic structure of this device was depicted in Fig. 3a, a layer of polyethylene terephthalate (PET) deposited with ITO electrodes on both sides formed the structural backbone of the triboelectric sensor (TES). A layer of fluorinated ethylene propylene (FEP) was applied on the top as an electrification layer for triboelectric charges generation by contact electrification with an external object. Vertically aligned polymer nanowires (PNWs) were created on the FEP layer (Fig. 3b) to achieve high sensitivity for low pressure detection. To characterize the response of the TES to a contact event, a square-shaped TES (Fig. 3c) was utilized to detect a metal object by cyclic contact and separation, which were realized through a linear motor. As shown in Fig. 3d, at a contact force of 20 mN (applied pressure of 0.03 kPa) the TES produced a uniform output voltage with the maximum amplitude of 35 V. As the contact pressure increased, the output voltage was raised to 50 V when the contact pressure approached 10 kPa (Fig. 3e). This increasing behavior could be attributed to the increase of contact area. It should be noticed that the curve in Fig. 3b exhibited two distinct regions, which was in agreement with the previous contact-mode active pressure sensor. In the extremely low-pressure region (<0.15 kPa), an exceptional pressure sensitivity of 44 mV/Pa was obtained with excellent linearity (R^2=0.991), corresponding to a sensitivity factor of 0.09% Pa^{-1}. In the relatively high-pressure region (>2 kPa), the pressure sensitivity dropped to 0.5 mV/Pa but still has good linearity (R^2=0.974). It was suggested that the two-region behavior was related to the enhancement effect from the PNWs. To further characterize the performance of the tactile sensor, the touch sensitivity depending on various factors such as the applied pressure, the size of the touching object, and the length of PNWs had been calculated and compared comprehensively. To demonstrate the practical application of this flexible and ultrasensitive tactile sensor, a complete wireless sensing system was developed through integrating the TES with a signal-processing circuit. The system relied on the output voltage from the TES to trigger an IC timer that controlled a wireless transmitter for remotely switching a siren alarm. As indicated in Fig. 3f, the sensing system immediately started operation once a human hand touched the door handle. Through substituting other functional electronics for the wireless transmitter in the circuit, the sensing system could be adopted for more purposes. For example, a touch-enabled switch for a panel light was successfully developed and shown in Fig. 3g. The TES in this work had a number of other unique advantages, including ultrahigh sensitivity, self-generated output, location independence, and outstanding robustness. In addition, the TES was generally applicable to objects made from various materials, indicating the widespread adaptability of the TES in a variety of circumstances. Therefore, the TES along with the sensing system developed here had immediate applications in a variety of areas, including human-machine interface, automatic control, surveillance, remote operation, and security systems.

Matrix of pressure sensors for self-powered tactile imaging

On the basis of the pressure/tactile sensors that were developed based on the contact-mode and single-electrode TENG, the sensor units could further be integrated into an array device for more advanced applications, like mapping the pressure distribution on a certain area, which would have potential applications for multiple fields like artificial skin, fingerprint recognition, electronic signature, etc. The first array of contact-mode triboelectric active sensors (TEAS) was developed by integrating a six-by-six matrix of the TEAS units onto the same grounded electrode [30], as shown in Fig. 4a. The measurement instrument was a voltage meter with an internal resistance of ~10 MΩ, and a corresponding voltage peak was recorded as response of a local pressure on the corresponding TEAS unit in the matrix. Once some of pixels in the array were pressed simultaneously, the voltage peaks would be only detected from those pixels, while the output profile of the other channels remained almost unchanged in the same time period. Based on this working principle, the tactile imaging capability of the TEAS matrix were demonstrated by loading pressure through pre-designed acrylic architecture with the calligraphy of the letters "TENG", respectively. Before applying the pressure, the voltage outputs from all the pixels of the TEAS matrix were at the background level, as displayed in Fig. 4b. Fig. 4c-f showed the two-dimensional contour plotting of the peak value of

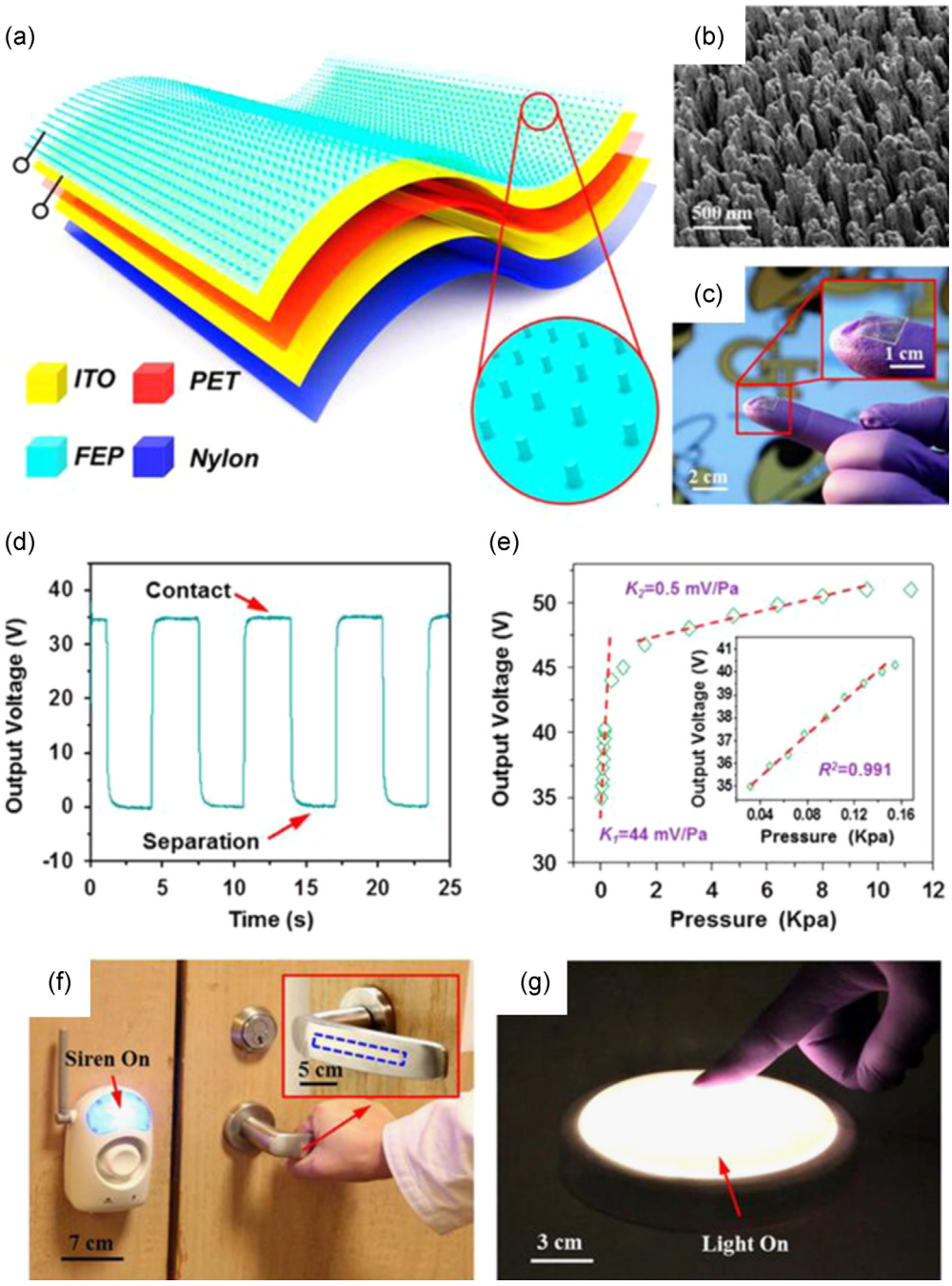

Fig. 3 The self-powered, flexible, and ultrasensitive tactile sensor. (a) The schematic structure of the tactile sensor. (b) The SEM image of the polymer nanowires created on the surface of the FEP thin film. (c) The photograph of the tactile sensor for measuring the contact event from a foreign object. (d) The measurement of open-circuit voltage with a cyclic contact force of 20 mN. (e) The summarized results of the output voltage under different contact pressures. Inset: an enlarged view of the summarized results at low pressure region. (f) A photograph showing that the TES was integrated with a signal processing circuit to turn on the siren alarm when a human hand touched the door handle. (g) A photograph showing that the TES was integrated with another signal processing circuit to turn on light when it was contacted by human fingers. Reproduced with permission from American Chemical Society [28].

the voltage responses that were measured when external pressures were applied through each architecture, respectively. The highlighted color represented the assembly of sensor units under pressing through each letter, as outlined by the white dash lines. These plots elaborated the spatial resolution of the TEAS matrix for distinguishable mapping of the applied pressure. Moreover, to gain a more intuitive understanding of the "self-powered" pressure mapping functionality of the TEAS matrix, each nine units of the same array device were connected in parallel to power up a serially-connected array of LEDs showing "T", "E", "N", "G" characters, respectively, which indicated that the sensor matrix could function as a stand-alone device without applying external power source.

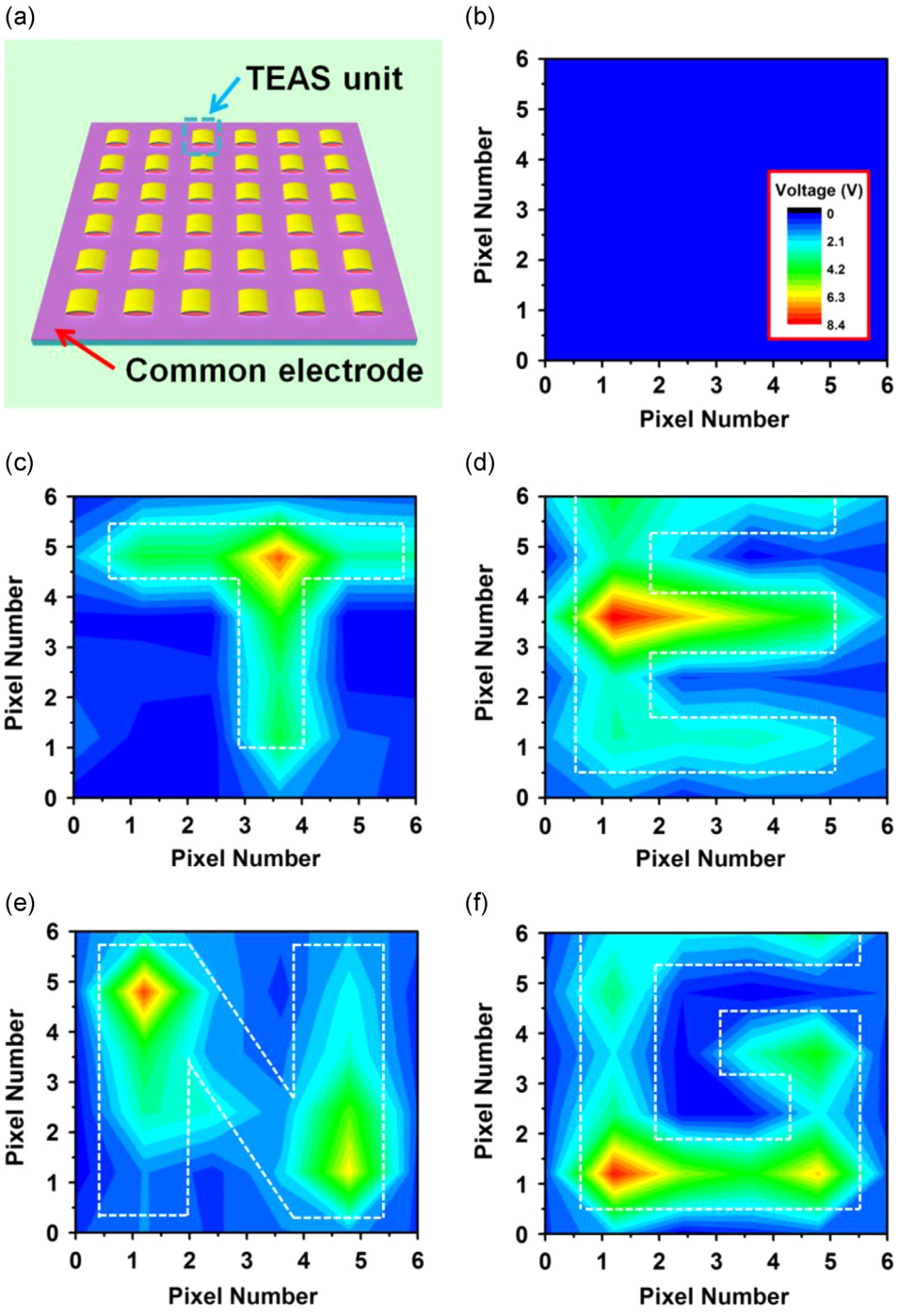

Fig. 4 Self-powered pressure mapping based on the TEAS array. (a) A schematic illustration of the TEAS array device. (b) The background signal with no pressure applied on the TEAS matrix. The inset is color scaling of voltage for all the measurements in this figure. (c–f) The two-dimensional voltage contour plot from the multi-channel measurement of the TEAS matrix with an external pressure uniformly and locally applied onto the device through architectures with calligraphy of "T", "E", "N", and "G", respectively. Reproduced with permission from American Chemical Society [30].

Similarly, the array of touch sensors based on single-electrode active sensors was also developed [29]. It was fabricated based on a piece of PDMS thin film and 8×8 array of separated ITO electrodes, which exhibited both transparent and flexible features. When the bottom, middle, and top areas of the matrix were touched by utilizing the side surface of the human hand, respectively, the output voltage signals can be detected from the corresponding pixels. To achieve the visualization of the pressure mapping, the triboelectric sensor array has been integrated with a printed circuit board composed of LED array accordingly [50]. The LEDs could be turned on locally when the back side of the sensor matrix was pressed, which reflects the spatial distribution of the applied pressure.

The most important features to be improved for the sensor matrix is the spatial resolution, which can possibly be

achieved through micro-fabrication and sophisticated design in the device structure.

Applications of TENG-based self-powered pressure/touch sensors for healthcare and security monitoring

Through innovative combination with different mechanical systems to detect pressure change and/or physical touch from different source, the basic concept and structure of the TENG-based self-powered pressure/touch sensors can be utilized for a variety of applications, such as healthcare and security. Several typical examples in this kind that has been demonstrated by our group are reviewed as follows.

The touch of a foreign object for the above described single-electrode TENG can be enabled by an air-pressure-controlled membrane. In this regard, a new membrane-based triboelectric sensor (M-TES) as a self-powered approach for air pressure change sensing, surveillance, and health monitoring (Fig. 5a) [53]. Having small dimensions of 3.7 cm by 3.7 cm by 0.2 cm and a light weight of 7 g, the M-TES can be utilized wherever the air pressure changes. High resolutions of 0.34 Pa and 0.16 Pa are achieved when the air pressure increases and decreases, respectively. Higher sensitivity can be obtained if the device is further miniaturized. As a result of the robust design, excellent stability is realized. Furthermore, the M-TES can effectively respond the pressure change caused by human footsteps, respirations and even heartbeats (Fig. 5b) without an external power supply. Therefore, the M-TES could have very broad applications in the fields of security surveillance, chemical engineering, geography research, and environment monitoring.

Besides, through utilizing the electrostatic charges on human skins for inducing the electrical signal generation, a flexible, reusable, and skin-friendly motion sensor for human—machine interfacing has been developed [54]. Based on triboelectrification, the as-fabricated device, relying on dry biopotential electrodes (Fig. 5c), is capable of accurately acquiring the real-time motion information from human joints. The periodic change of contact areas between human skin and polydimethylsiloxane (PDMS) establishes electric potential difference, and thus brings into charge transfer between the copper electrode and the ground. Functioned as a self-powered human motion sensor, the entire device is consisted of an array of independently addressable units, which can record the electric output signals as a mapping figure to transmit the kinematic information on human joints (Fig. 5d). The motion sensor arrays produced an open-circuit voltage as high as 42.6 V with a remarkable signal-to-noise ratio (SNR) of higher than 1000, which guarantees the superior sensitivity and selectivity of the devices as sensors to accurately record and impart the motions of the human joints, such as elbow, knee, heel, even finger. This study shows a possibility of utilizing triboelectrification based and self-powered motion sensor system for HMI.

Moreover, through utilizing paper as the skeleton materials, a new type of TENG has been demonstrated, which can be incorporated in a book or any other paper product with the advantages of transparent and flexible [55]. Such paper-based TENGs can generate electricity when the sheets of papers come into contact, bend or slide relative to one another, and having the advantages of being both transparent and flexible. In addition, we also integrate grating-structured PTENGs into a book as a self-powered anti-theft sensor (Fig. 5e). The mechanical agitation during handling the book pages can also be effectively converted into an electrical output (Fig. 5f) to either drive a commercial electronic device or trigger a warning buzzer (Fig. 5g). Furthermore, different grating structures on each page produce different numbers of output peaks, which can accurately position the turned pages and record the number of pages turned. This work provides a potential method to develop a self-powered, durable, cost effective anti-theft system for books, paintings and any other flexible materials in the future.

Triboelectric nanogenerators as self-powered active vibration sensors

Vibration is one of the most important forms of mechanical motions that can be found in ambient environment, such as the vibration motions of engines, vibrations in buildings and bridges, the shaking of a flying aircraft, and ocean wave oscillations. Since the vibrations can directly reflect the operation status and the health of machineries and infrastructures, the sensing of vibrations is of critical importance in equipment maintenance and environment monitoring. Up to date, various transducers have been fabricated for monitoring and detecting vibrations and impacts [56–58]. As an effective approach to convert vibrational motions into electricity, the TENGs can also serve as the self-powered active sensors for vibrations [35,36,41,50]. Among the several basic modes of TENGs, the vertical contact motion based operation modes – the vertical contact-separation mode and the contact-based freestanding mode – are particularly suitable for this purpose. Based on these two working modes, several different self-powered active vibration sensors have been developed with different characteristics and functionalities, such as the positioning of vibration sources [41,42] and quantitative detection of vibration amplitude and frequency [50].

Contact-mode TENGs as self-powered active vibration and positioning sensors

The vertical contact-separation mode TENG generate electricity through the periodic contact and separation between the two triboelectric layers, which is generally enabled by the vertical-to-plane vibrational motion of at least one of the two plates in the TENG. Thus, through integrating the typical structure of the contact-mode TENG into an unstable mechanical structure that can self-balance under perturbation, the constructed device can not only harvest energy from vibrations, but also serve as a self-powered vibration sensor. Among these structures, the 3D spiral structure is a typical example [41]. It is a three-dimensional curve around an axis at a continuously reducing radius while moving parallel to the axis, which can be simply regarded as a conical shaped spring structure. Loaded with a seismic mass, the suspended 3D spiral structure can oscillate as a

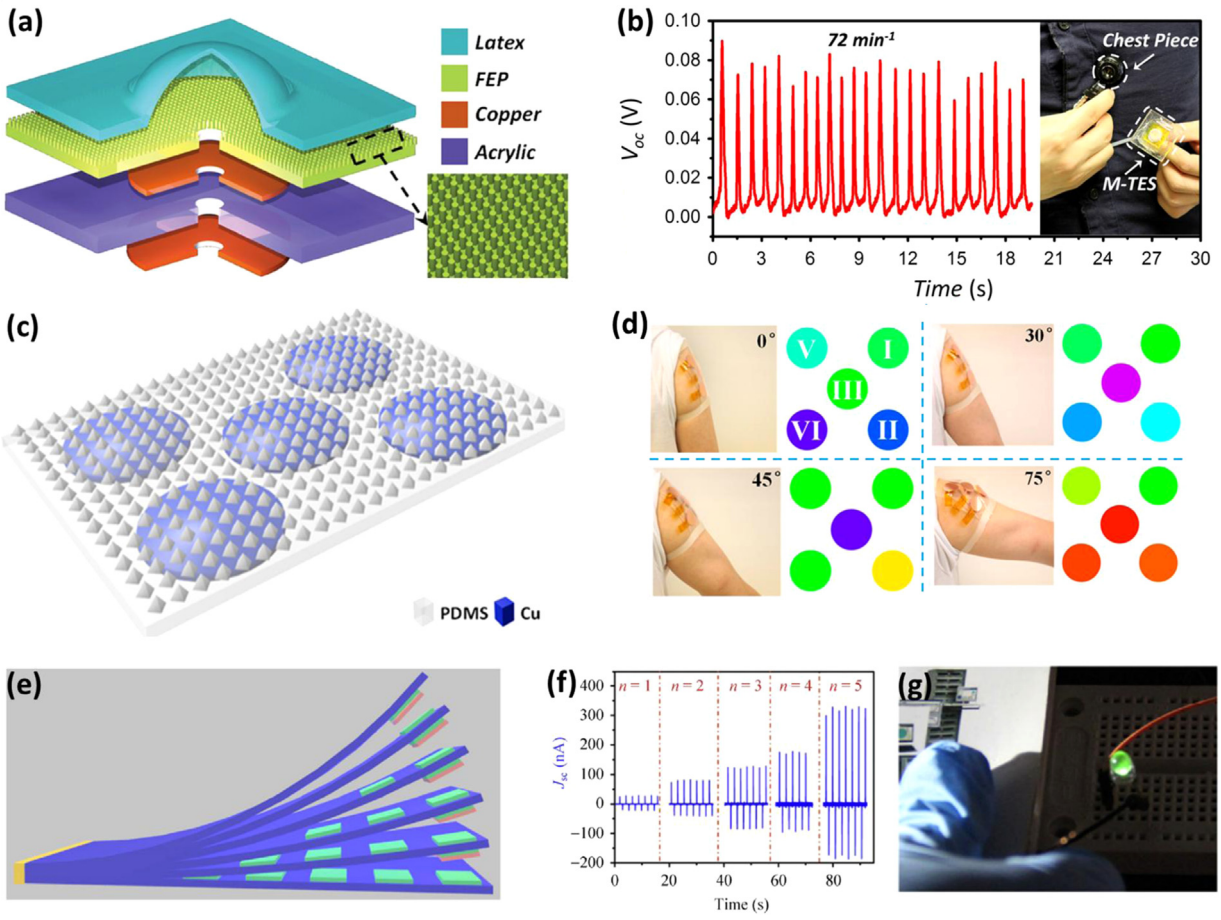

Fig. 5 TENGs as self-powered touch/pressure sensors for applications in healthcare and security monitoring. (a) Schematic of the membrane-based self-powered triboelectric sensors (M-TES) for pressure change detection with applications in security surveillance and healthcare monitoring. (b) Demonstration of the M-TES as a heart beating monitor. (c) Schematic of the TENG-based motion sensor for human–machine interfacing. (d) Electrical measurement results of the TENG-based motion sensors array when it was mounted on the human shoulder joints undergoing an up-down motion of upper arm. (e) Structure of the TENG sensor integrated in a book. (f) Electrical signals generated by the sensor under the simulated action of stealing a book. (g) Photograph showing that the electrical signal generated by the sensor triggers an LED as a warning buzzer. Reproduced with permissions from Wiley, American Chemical Society, and Springer [53-55].

response to external disturbance at a high sensitivity. A spiral TENG (STENG) that operates in the contact-mode was built at the front of the seismic mass in a spiral structure. The spiral structure behaves like a spring in response to an external disturbance. A schematic diagram of the STENG is shown in Fig. 6a. An acrylic sheet is chosen as the structural material. The working parts that generate the electricity are two round plates facing each other, which is marked in Fig. 6a with a red dashed line. One is attached at the bottom of the 3D spiral structure. The other one is centered and fixed on the upper surface of the cube's bottom. The height of the cube was adjusted to have these two plates be in slight contact when the spiral is relaxed and in equilibrium. The upper contact surface is an aluminum film coated on an anodic aluminum oxide (AAO) template. The lower contact surface is a Kapton film. The surface of the Kapton film was modified to introduce aligned nanowire structures. The nanostructures on both the surfaces can increase the surface roughness and the effective surface area of the STENG for effective triboelectrification. When the STENG is working, the spiral oscillates in response to an external vibration source, so that the distance between the Al and Kapton film changes. During this process, the electricity is generated following the principle of contact-mode TENG.

The STENG can serve as self-powered active sensors for vibration detection and monitoring. This means that whenever there is a vibration disturbance in the environment experienced by the STENG, the STENG will be triggered to generate an indicating electric signal. As in some situations vibrations are undesirable and harmful, in addition to vibration detection, the vibration source positioning is very important and of great practical value. Here, the STENGs were used to construct a multichannel active sensor system, and the in-plane vibration source positioning was realized. The vibration source positioning test was carried out on a wood board with dimensions of 1 in. × 24 in. × 48 in. Three STENGs were positioned on three corners of the board, as shown in Fig. 6b. A three-channel measurement was applied to acquire data from these three STENGs simultaneously. A representative signal pattern is shown in Fig. 6c, which was acquired when the small hammer hit position 7. Because

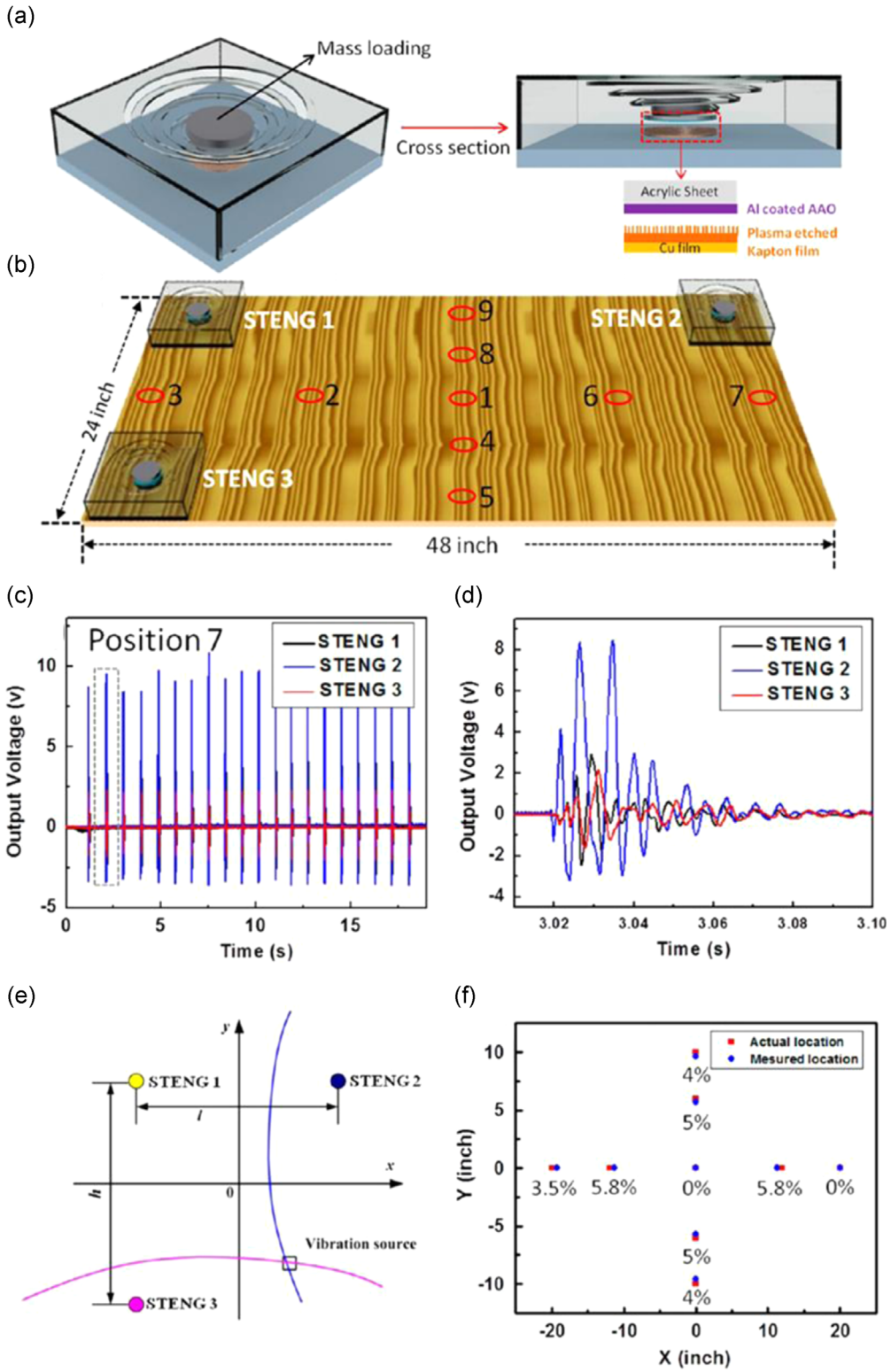

Fig. 6 3D-spiral triboelectric nanogenerator as a self-powered vibration sensor. (a) Schematic diagram of the device and its cross section view. (b) Schematic diagram of the experimental setup showing three STENGs positioned at the three corners of a wood board for the detection of a vibration source. (c) Recorded signal patterns when the impact is located at position 7. (d) Enlarged view of one peak signal in (b), which is indicated by a dashed gray rectangle. (e) Schematic diagram of the principle to locate the vibration source. (f) Comparison of the measured location and actual location of the vibration source and corresponding location error. Reproduced with permission from American Chemical Society [41]. (For interpretation of the references to color in this figure legend, the reader is referred to the web version of this article.)

STENG 2 is the closest one to the vibration source, it obtains the highest signal level. For STENG 1 and STENG 3, the signal levels are similar due to the equal distance from the vibration source. Fig. 6d is the enlarged view of one signal peak in Fig. 6c, which is indicated by a dashed gray rectangle. The vibration propagated and first arrived at STENG 2 and then arrived at STENG 1 and STENG 3 at the same time. Thus the first signal peak from STENG 2 is earlier than the two from STENG 1 and STENG 3. The principle to locate the vibration source is depicted in Fig. 6e. We can obtain the arrival time differences of the signal among the three STENGs. Combining the vibration propagation speed, we can get information on the distance difference from the vibration source to STENG 1 and STENG 2 (D1), as well as the distance difference from the vibration source to STENG 1 and STENG 3 (D2). The track of an object that maintains the same distance difference from two fixed points is a hyperbolic curve, as indicated by the blue and purple curves in Fig. 6e. The vibration source is located at the intersection of the two hyperbolic curves by solving a set of equations. The corresponding experimental results are shown in Fig. 6f. The position at the center of the board is accurately located without error, and the location error for other positions is less than 5.8%. This error can be improved by increasing the sampling rate of the data acquisition equipment.

Besides the 3D-spiral-based TENG, several other structure designs of the contact-mode TENG have been developed for harvesting vibrational energy, such as the harmonic-resonator-based TENG [35], the 3-D TENG with broadband response [42], the 3-D stack integrated TENG [59], the triple-cantilever-based TENG [60], and the integrated rhombic gridding based TENG [43]. They all can be utilized as the self-powered active sensor to detect external vibrations.

Freestanding-mode TENG as self-powered active vibration sensors for quantitative amplitude measurement

Generally, vibrations are characterized by two parameters: frequency and amplitude. The vibration frequency can be easily quantified by most vibration sensors, but a quantitative measurement of the amplitude is relatively more difficult because it often requires a linear relationship between the sensing signal and the amplitude. The above described several demonstrated TENG structures for vibration applications based on the vertical contact-separation mode is only applicable for measuring the frequency but not the amplitude. This is because that the electricity generation behavior of the vertical contact-separation mode is not linear to the separation distance, due to the nature of the changing capacitance between the two electrodes during its operation. Among the four fundamental modes for TENGs, the freestanding-triboelectric-layer mode has stationary electrodes thus constant electrode capacitance. Based on this mode, a contact-separation-enabled freestanding-TENG (CF-TENG) has been proposed, in which the vibration of the freestanding triboelectric layer between the two electrodes periodically changes the induced potential difference between the two electrodes and thus generate electricity in external load. In such a structure with the electrodes' lateral dimension much larger than their vertical separation distance, the electricity generation has a linear relationship with the moving distance of the freestanding layer [50].

The structural design of the vibration-enabled CF-TENG is schematically shown in Fig. 7a. Its skeleton is constructed by laser-cut acrylic sheets. Two Al-deposited acrylic plates are supported in a face-to-face configuration serving as the two stationary electrodes of the CF-TENG. In between, another acrylic sheet is employed as the vibration resonator in the CF-TENG through having its four corners connected by 8 springs to the two ends of the acrylic skeleton. Two FEP films as the freestanding triboelectric layers are laminated onto the two sides of this acrylic sheet. They have the same size with the electrode. Triggered by the external vibration source that the CF-TENG is attached to, the two triboelectric layers are brought by the resonating acrylic sheet to alternatively approach the two electrodes in a vertical-to-plane manner. When its vibration amplitude is large enough, the contact between the FEP layer and the Al surface will generate triboelectric charges. In order to further enhance the triboelectric charge density, the FEP surface is etched by the ICP reactive ion etching to create the nanowire-structures (Fig. 7b). As shown in the SEM image (Fig. 7c), these vertically-aligned nanowires have an average diameter of $\sim$100 nm and a length of $\sim$1 μm.

When the CF-TENG with the resonator plate supported by springs is bonded to a vibration source, the resonator plate will be triggered to vibrate between the two electrodes. The linear characteristic gives the CF-TENG the supreme capability of quantitatively sensing the amplitude of the vibration. When the frequency was at the resonant frequency of the CF-TENG (Fig. 7d), both the peak-to-peak value of the V_{OC} and the amplitude of the I_{SC} increase almost linearly with the increase of the vibration amplitude, as long as it within the small range (below 1.5 mm, i.e. Region I shown in Fig. 7d). This response comes from the linear relationship between the agitated vibration amplitude of the resonator plate and the vibration amplitude of the entire CF-TENG. However, when the vibration amplitude is above $\sim$1.5 mm, the resonator plate will start to get into contact with the two electrode plates. This results in the saturation behavior of the electrical outputs in Region II shown in Fig. 7d. Moreover, from Fig. 7e as the enlarged plot of the curves in Fig. 7d below the vibration amplitude of 0.3 mm, it can be found that both the V_{OC} and the I_{SC} have very good linear responses. When the vibration amplitude is only 3.5 μm, the peak-to-peak value of the V_{OC} and the amplitude of the I_{SC} generated by the CF-TENG still have 0.54 V and 10 nA. Therefore, when the vibration source is at or close to the resonant frequency of the CF-TENG, it has an extremely high sensitivity for very subtle vibrations. In the other group of experiments with the frequency at 21 Hz, which is off the resonant frequency (Fig. 7f), when the vibration amplitude is increased up to 15 mm, both the V_{OC} and the I_{SC} follow very good linear behaviors. Thus, when the vibration source is not at the resonant frequency of the CF-TENG, this active sensor has the capability of quantitatively measuring the amplitude in a wide range.

As a demonstration of the CF-TENG's outstanding capability in vibration sensing, it was mounted onto a wind blower to monitor its vibration during the operation (Fig. 7g). When the wind blower was sequentially turned

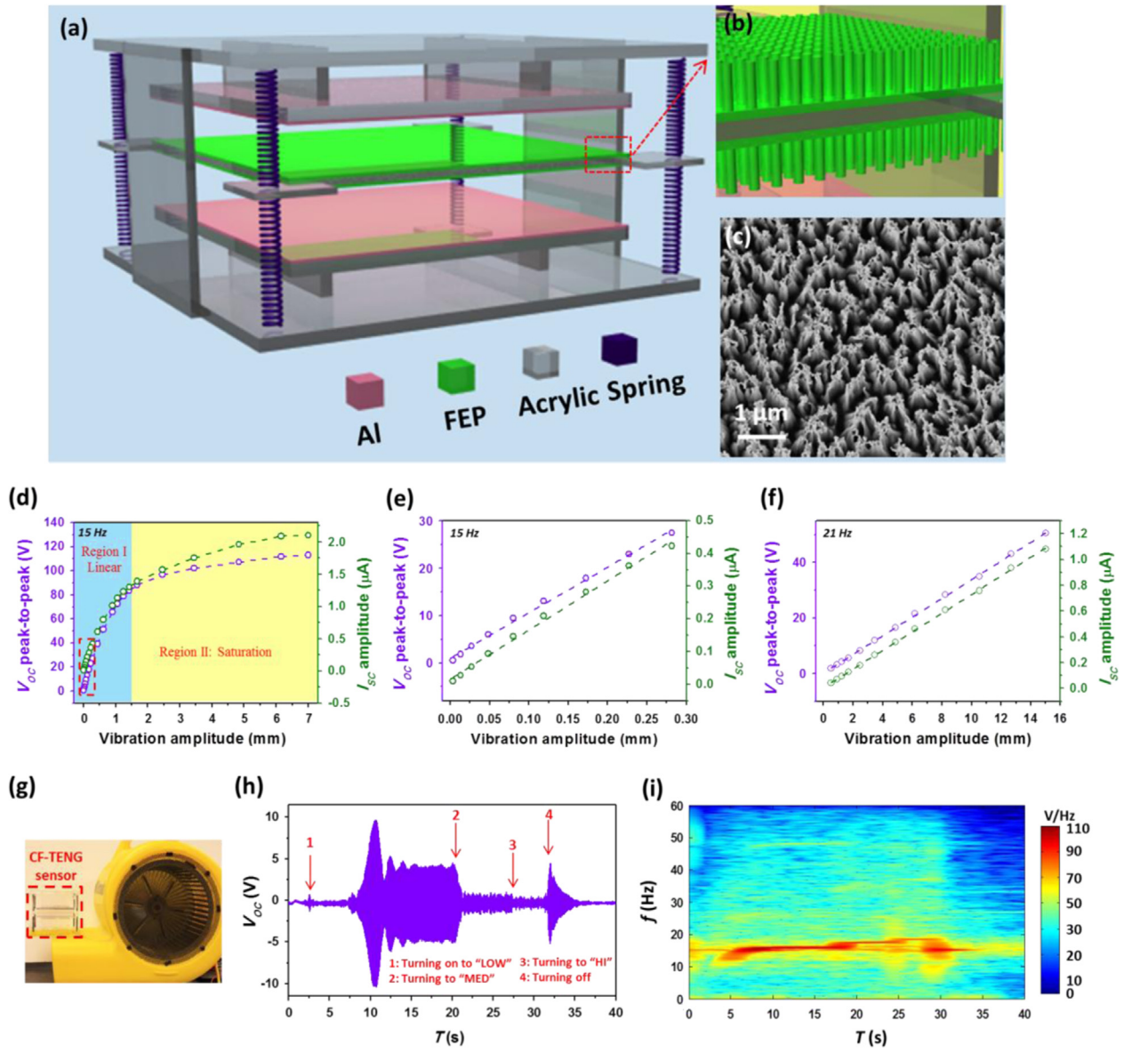

Fig. 7 Contact-mode freestanding TENG as self-powered vibration sensors for quantitative amplitude measurement. (a) Schematic diagram showing the typical device structure of a CF-TENG. (b) Enlarged view of the device structure showing the nanowire-structure on the surface of the FEP films attached on the resonator plate. (c) SEM image of the nanowire structures on the FEP films. (d) V_{OC} and I_{SC} from the CF-TENG triggered by vibrations with different amplitudes, when the external vibration source is at the resonating frequency (15 Hz) of the CF-TENG. (e) Enlarged plot of Fig. 4d with the vibration amplitude in the range below 0.3 mm. (f) V_{OC} and I_{SC} from the CF-TENG triggered by vibrations with different amplitudes, when the external vibration source is not at the resonating frequency of the CF-TENG. (g) Photograph showing the demonstration of using the CF-TENG to monitor the vibration of a wind blower during its operation. (h) V_{OC} from the CF-TENG when the wind blower was sequentially switched to different speeds. (i) Short-time Fourier transform of the V_{OC} signal shown in Fig. 6h. Reproduced with permission from American Chemical Society [50].

on from the "off" state to the "LOW" speed, then turned to the "MED" speed, then to the "HIGH" speed, and finally turned off, the V_{OC} signal generated by the CF-TENG is shown in Fig. 7h. From the short-time Fourier transform (STFT) of the V_{OC} signal, the instantaneous frequency distribution of the wind blower throughout this operation process can be obtained in Fig. 7i. In each stage with the same frequency, the change of the amplitude in the V_{OC} signal directly reflects the change of the vibration amplitude of the wind-blower, as shown in Fig. 7h. Therefore, this demonstration convincingly shows the CF-TENG's supreme capability in quantitatively detecting both the amplitude and the frequency of any arbitrary vibration.

Contact-mode TENGs as self-powered active acoustic sensors

Acoustic wave is a special form of vibration ubiquitously existing in the environment, which appears in a wide range

of frequency and strength. The sensing of acoustic waves is very important not only for information technology, but also for the monitoring of equipment systems and environment. With the possibility of converting sound waves into electricity, TENGs could provide an effective approach for realizing the self-powered acoustic sensing.

The first organic thin-film based triboelectric nanogenerator (TENG) has been developed to not only scavenge ambient acoustic energy as a sustainable power source, but also measure the acoustic waves as a self-powered active acoustic sensor in the low frequency range available in our daily life [36]. By utilizing a Helmholtz cavity, the sensitivity of the as-fabricated device was as high as 9.54 V/Pa in the acoustic pressure range from 70 dB_{SPL} (0.063 Pa) to 110 dB_{SPL} (6.32 Pa), and the directional pattern is in a shape of Cardioid with a total response angle of 52°. This acoustic TENG relies on a Helmholtz cavity with a size-tunable narrow neck on its back. The core part of the nanogenerator is in a circular shape and embedded as the flexible front plate of the cavity, as schematically shown in Fig. 8a. For a better illustration, a cross-sectional view of the core is shown in Fig. 8b, with a multilayered structure. Aluminum thin film with nanoporous surface plays dual roles as an electrode and a contact surface. The SEM image of the nanopores on the aluminum is shown in Fig. 8c. On the counter side, a layer of PTFE film with deposited copper was employed as another electrode. An SEM image of the PTFE nanowires is displayed in Fig. 8d. When an external sound wave is incident on the core part of the TENG, the air within the cavity gets alternately compressed and expanded, with the resulted pressured difference related to the magnitude and frequency of the sound wave. As a result, the PTFE thin film will oscillate due to the initiated pressure difference on its two sides while the aluminum film stays still.

With a superior capability in converting acoustic waves into electricity, this TENG can also act as an active self-powered acoustic sensor for different applications. The demonstrated application is to use the acoustic TENG as a self-powered microphone. The natural frequencies of the devices can be purposely tuned by the structural parameters configuration. Thus, we can have their corresponding frequency bands overlap with each other to give a broadened working bandwidth. Here, as demonstrated in Fig. 8e, four nanogenerators, NG_1, NG_2, NG_3, and NG_4, respectively, with a series of dimensions corresponding to resonance frequencies of 350, 650, 1100, and 1400 Hz, respectively, were employed to widen the overall working bandwidth from 10 Hz to 1700 Hz, which enabled the superior performance of the TENG as a self-powered microphone for sound recording. Parts f1 and f3 of Fig. 8 are, respectively, the time domain waveforms of the recorded sounds from NG_1 and NG_4. Although NG_1 and NG_4 were triggered by the same sound source, the waveforms of the two apparently exhibit different characteristics, which is attributed to a different frequency response ranges of the two. With a natural frequency of 350 Hz, the waveform of NG_1 is smoother owing to its dominant response to lower frequency components from 10 Hz to 600 Hz, as shown in Fig. 8f2, which is the corresponding short-time Fourier transform (STFT), while the waveform of NG_4 with a natural frequency of 1400 Hz is rougher, due to its dominant response to the higher frequency components from 1100 Hz to 1700 Hz, as demonstrated in Fig. 8f4 of its corresponding STFT. In order to reconstruct the original sound, the acquired acoustic signals of the array are weighted according to the relative amount of information available from each source. The waveform of the reconstructed signal and its corresponding STFT are illustrated in parts g1 and g2, respectively, of Fig. 8. The frequency components of the reconstructed signal cover all the frequencies ranging from 10 Hz to 1700 Hz, as demonstrated in Fig. 8g2. Fig. 8d shows an as-fabricated TENG working as a self-powered microphone for sound recording. In another demonstration of the acoustic TENG for the sensing purpose, it acts an acoustic source localization sensor. Experimentally, three as-fabricated TENGs were arranged in an L shape and anchored in a 2D plane with dimensions of 2 m by 1.8 m. The results show that positioning within an average error circle of 7 cm in diameter is achieved based on multiple measurements.

The proposed acoustic sensors in this work have extensive applications in fields such as military surveillance and reconnaissance, intruder detection, sniper localization, underwater acoustics, and auto talker detection in a web conferencing.

Triboelectric nanogenerators as self-powered active motion sensors

Mechanical motions are generally characterized by a series of parameters, such as movement distance, velocity, accelerations, and angles. Sensors for the monitoring and detection of these parameters for the mechanical motions are vitally important for a lot of mechanical systems. With different structural designs, triboelectric nanogenerators have been developed to generate electricity from different types of mechanical motions, such as linear sliding and rotation [34,61]. Since the frequency, the amplitude and the total periods of the generated electrical signals are all directly related to the parameters of the input mechanical motions, the TENGs can serve as self-powered active motion sensors. Even if such motions are in concealed locations, TENGs can be utilized to track the trajectory and detect the instantaneously parameters of the motions.

TENGs as self-powered linear displacement sensors

Measurement of displacement and speed at the micro- and nano-scale has ubiquitous applications in the scientific and industrial fields such as manufacturing, automation, robotics, and nano-manipulation. Most of the existing sensing technologies need pre-provided electrical or optical signals in order to detect the mechanical displacement, which inevitably requires external power sources. However, the increased number and density of portable electronic devices and sensing networks today desperately desires low power consumption and/or self-powered sensors. Based on the triboelectric nanogenerators, a self-powered, one-dimensional displacement and speed sensing technology has been demonstrated, which achieves high resolution, large dynamic range and long detecting distance [61].

The motion sensor consists of two micro gratings with identical patterns, as sketched in Fig. 9a. The grating at the

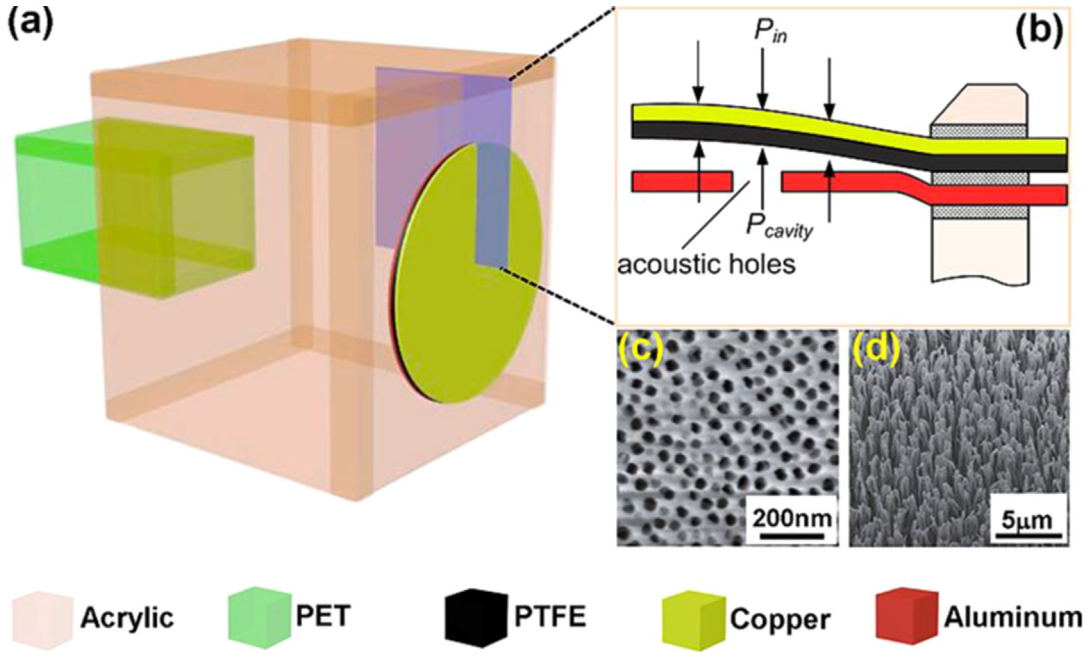
(a)
(b)
P_{in}
P_{cavity}
acoustic holes
(c)
200nm
(d)
5μm
Acrylic
PET
PTFE
Copper
Aluminum

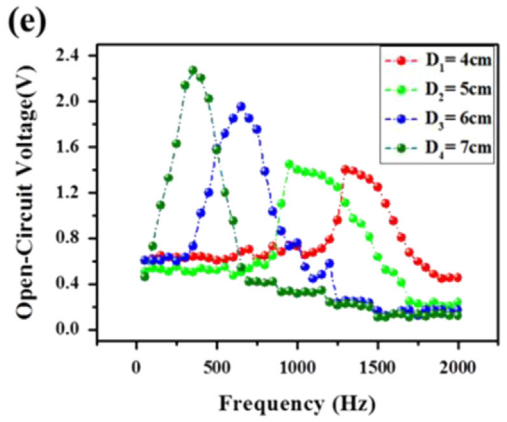
(e)
Open-Circuit Voltage(V)
Frequency (Hz)
D_1= 4cm
D_2= 5cm
D_3= 6cm
D_4= 7cm

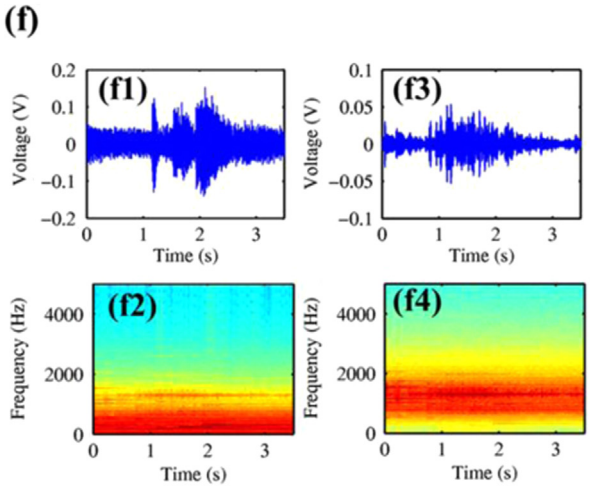
(f)
(f1)
(f2)
(f3)
(f4)
Voltage (V)
Frequency (Hz)
Time (s)

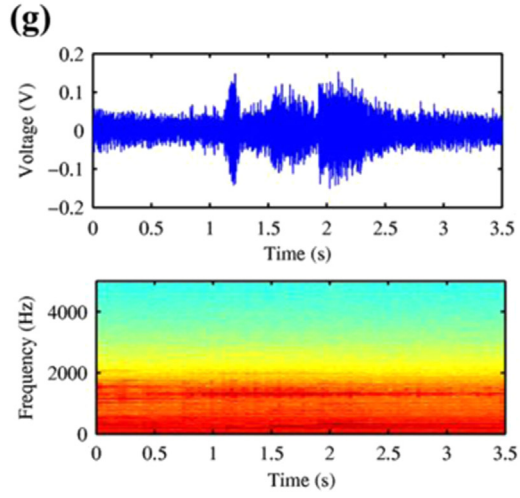
(g)
Voltage (V)
Frequency (Hz)
Time (s)

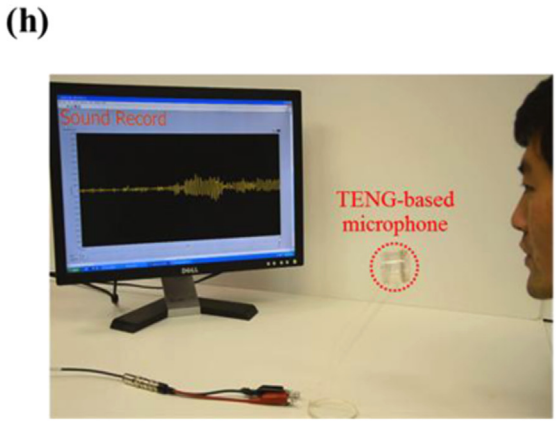
(h)
Sound Record
TENG-based
microphone

bottom is made of an etched silicon wafer coated with aluminum as the bottom electrode and silicon dioxide as triboelectrically positive material; the grating on the top is made of patterned SU-8 film on a glass slide as supporting substrate and subsequently coated with ITO and Parylene film as the top electrode and triboelectrically negative material, respectively (Fig. 9a inset). The detailed microscopic structure of the as-fabricated devices are shown in Fig. 9b and c, respectively. The relative motion between two gratings leads to periodic separation of two micrograted dielectric materials that are oppositely charged through triboelectrification. As a result, an alternating electric signal between the metal electrodes placed beneath the dielectric materials can be detected due to electrostatic induction.

During the movement, the OC voltage measured between the two electrodes (Fig. 9d) alternates between 0 and ~160 mV periodically. As aforementioned, since each cycle corresponds to one period of the gratings, which is 200 μm in this device, the real time displacement can be calculated by accumulating extra 200 μm once one more peak is detected. As shown in the blue curve in Fig. 9e, the detected displacement increases linearly with time. With time frame simultaneously recorded, the real time motion speed can also be derived by dividing the width of one pitch (200 μm in this device) by the time interval between two adjacent voltage peaks. Investigation on the voltage within a period can substantially enhance the resolution in displacement detection. Starting from a status with complete overlap, a step motion test with each step of 5 μm was performed. The sensitive region is found to be from 10 μm to 190 μm, where each step motion of 1 μm can be clearly differentiated from the voltage response, as shown in Fig. 9f. The change of the voltage for each step is about 2.2 mV, and the Root Mean Square (RMS) of the noise V_{noise} at 1 Hz is 0.38 mV. Consequently, the displacement resolution at bandwidth of 1 Hz can be calculated to be 173 nm.

The measured SC current can also serve as the sensing signal for the displacement distance and the speed. Since the I_{SC} is alternating between negative and positive periodically during the motion, as displayed in Fig. 9g, the real time displacement can be derived (shown by the blue dots in Fig. 9h) by counting the number of zero-crossings, each of which counted as 100 μm step of displacement. Compared with the preset trajectory as indicated in red curve, the measurement matched very well. On the other hand, the amplitude of the I_{SC} can also help to quantitative determine the real time speed, given small aspect ratio of the insulating layer. Fig. 9i shows the plot of the magnitude of the detected current against motion speed from 5 μm/s to 10 mm/s and a linear fit that gives its sensitivity of (679 ± 4) pA/(mm s^{-1}) with adjusted $R^2 = 0.99938$. The resolution in dynamic speed detection is calculated to be 1.2 μm/s, given the RMS value (0.8 pA) of the noise.

The resolution for both displacement and speed sensing can be further improved by reducing the grating period. This new approach for displacement/speed sensing distinguishes itself from the existing technologies by a combination of self-powered, nanometer resolution, long detecting range and non-optical compacted structure, showing extensive potential applications in automation, manufacturing, process control, portable device, etc.

Besides, based on the single-electrode TENG, a self-powered displacement sensor has been developed through using grated linear row of Al electrodes for detecting the motion of an object without the use of an external power source [46]. The output voltage signals from 16 Al electrode channels were recorded in real time as a mapping figure. The motion direction and location of the object can be obtained by the analysis of the measured mapping figures.

TENGs as self-powered active rotation sensors

On the basis of the lateral-sliding mode of TENGs, a disk TENG with segmental structures for harvesting rotational mechanical energy has been demonstrated [21]. The electricity can be generated from rotations through cyclic in-plane charge separation between the segments that have distinct triboelectric polarities. Enabled by the distinct relationship between the electrical output (its frequency and amplitude) and the rotational speed, the disk TENG can also serve as a self-powered angular speed sensor for rotation motions.

Later on, a free-rotating disk TENG (FRD-TENG) has been developed based on the freestanding-triboelectric-layer mode, which could also be employed as a self-powered rotation sensor for simultaneously detecting the rotation speed and vertical displacement [34]. Due to the unique advantages provided by the freestanding-triboelectric-layer mode, the FRD-TENG can operate in non-contact mode, and the rotating part doesn't need to have a lead extended out. As schematically illustrated in Fig. 10a, the basic structure of the FRD-TENG were composed of the freestanding rotational part of tribo-charged layer, and the stationary part of metal electrodes. The rotational part was fabricated from a piece of fluorinated FEP thin film that was tailored into a four-segment structure. The stationary part is composed of two sets of complementary aluminum electrodes with similar four-segment structures. To increase the

Fig. 8 Triboelectric nanogenerator for self-powered active acoustic sensing. (a) Sketch and (b) cross-sectional view showing the structural design of the triboelectric nanogenerators. (c) SEM image of nanopores on aluminum electrode. (d) SEM image of PTFE nanowires fabricated on the film surface by plasma etching, which largely increase the triboelectrification. (e–h) Demonstration of the TENG acting as a self-powered microphone. (e) Frequency responses from the nanogenerators array, which consists of four NGs with various designed natural frequencies, aimed to enhance the overall working bandwidth. (f1 and f2) Sound waveforms of the signals acquired byNG1 and NG2, respectively. (f3 and f4) Short-time Fourier transforms of the acquired signals by NG1 and NG2, respectively. (g) Sound waveform and corresponding short-time Fourier transform of the signals acquired by the array of the NGs. (h) Photograph that shows a NG is working as a self-powered microphone for sound recording. Reproduced with permission from American Chemical Society [36].

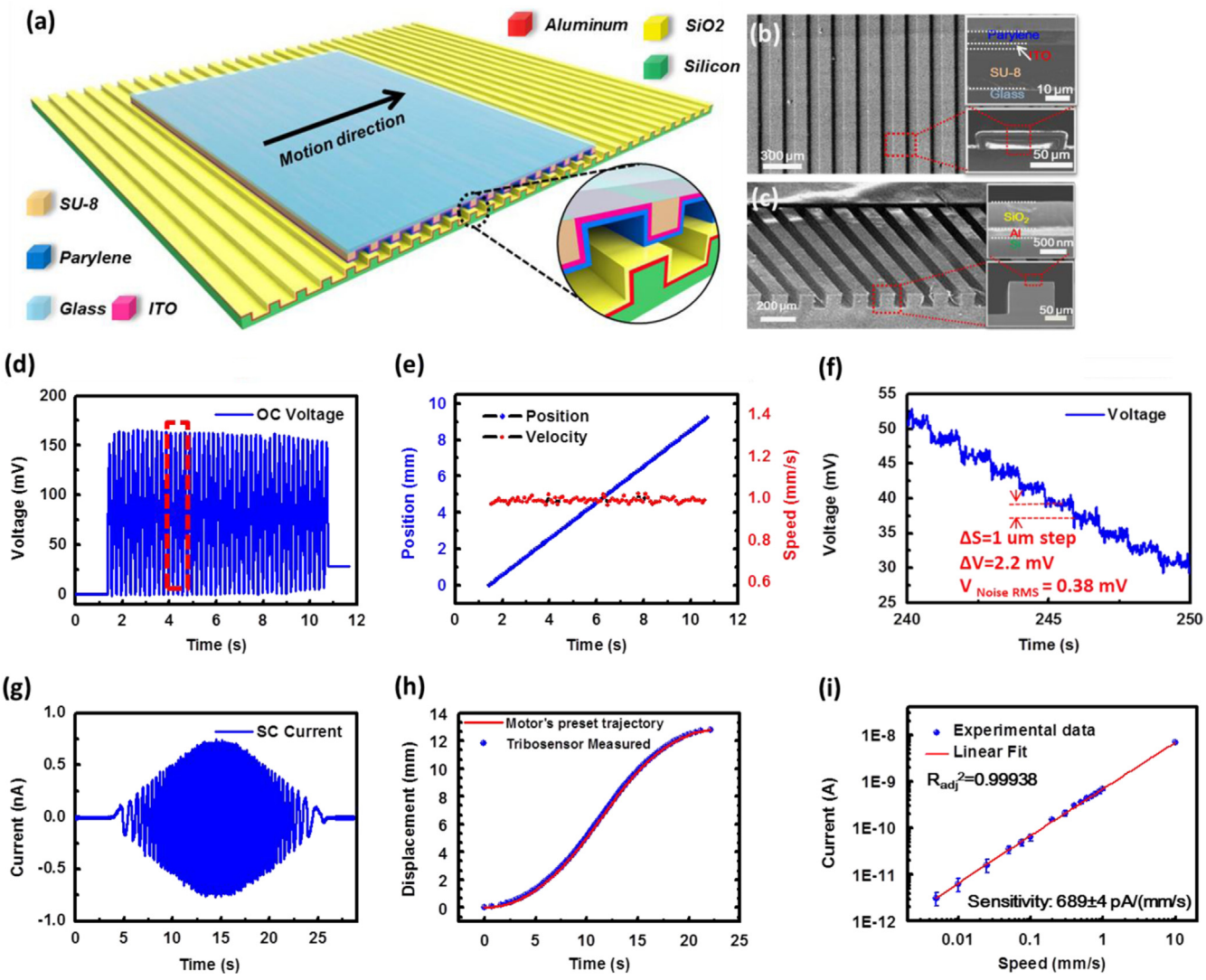

Fig. 9 Micro-grated triboelectric nanogenerator as nanometer resolution self-powered linear displacement sensor. (a) Schematic showing the structure of a TENG-base self-powered displacement sensor, with a pair of micrograting, the inset illustrates the detailed information of layers. (b) SEM images of the top micrograting with glass slide substrate. The insets show the cross section: the ITO layer on top of the patterned SU-8 photoresist serves as the top electrode, and the outmost layer is Parylene film serving as electronegative triboelectric layer. (c) SEM images of the bottom micrograting. The insets show the cross section profile: the etched Silicon is coated with Al as bottom electrode and SiO_2 as electropositive triboelectric layer. (d) The OC voltage signals acquired from a displacement of 9.2 mm at a preset speed of 1 mm/s. (e) The real time displacement and speed derived from the measured voltage signal. (f) Step motion with 1 μm per step in the sensitive region (10–190 μm) can be clearly resolved through the OC voltage signal. Given the RMS value of noise (0.38 mV), and the voltage change corresponding to 1 μm step motion (2.2 mV), the resolution can be calculated to be 173 nm. (g) The SC current signals acquired from a non-uniform motion (decelerate – uniform speed – deceleration). (h) The preset motor's trajectory and the real time displacement detected by the motion sensor. (i) A plot of SC current as a function of motion speed from 5 μm/s to 10 mm/s with a fitted sensitivity of 689 ± 4 pA/(mm s^{-1}). Reproduced with permission from Wiley [61].

tribo-charge density, micro-patterned structures were introduced on the inner surface of both triboelectric layers, respectively (Fig. 10b and c). The two triboelectric layers were first brought into contact to produce triboelectric charges, and then brought apart with non-contact rotation to induce potential difference between the two aluminum electrodes. The potential would serve as the driving force for the charge flow in the external load to produce output current. Both the rotation speed (r) and the vertical distance (d) have impact on the output performance of the FRD-TENG, so that it could then be employed as self-powered sensor for the active detection of the two parameters.

To elucidate its impact of the vertical separation distance (d), the output performances of the FRD-TENG under a series of distances increasing from 0 to 5 mm were measured at a constant rotation speed of 500 rpm. The measured J_{SC} shows a decreasing trend from 2.0 mA/m^2 to 0.5 mA/m^2, due to the reduction of electrostatic induction from the negatively-charged FEP layer. This relationship implied that the FRD-TENG could be employed as a

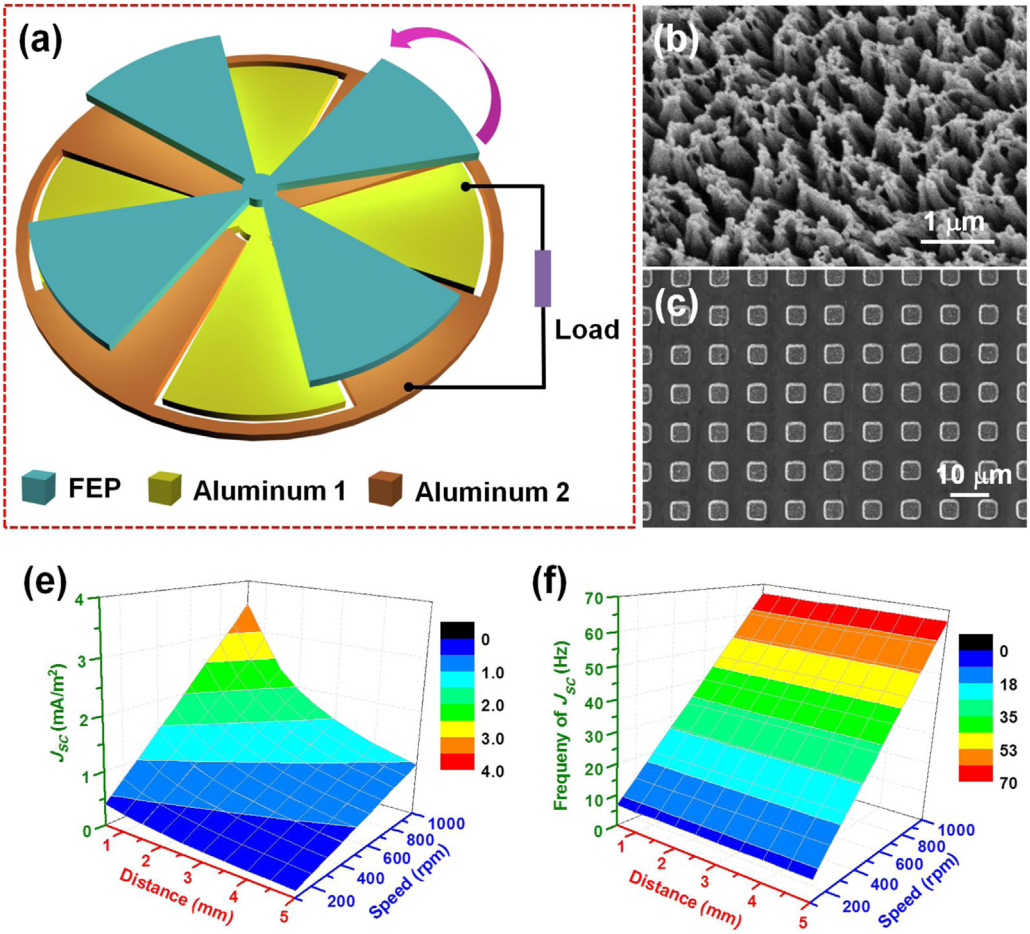

Fig. 10 Self-powered vertical displacement and rotation speed sensor based on the free-rotating-disk triboelectric nanogenerator. (a) The schematic of the basic structure of the FRD-TENG composed of the freestanding FEP layer and the stationary aluminum layer. The bottom inset is the figure legend. (b) A 30°-tilted-view SEM image of the nanorod structure created on the surface of the FEP thin film. (c) A top view SEM image of the cubic micro-patterned structures on the aluminum foil. (d) A three-dimensional plot of the magnitude of the J_{SC} depending on variable vertical displacements and rotation speeds. (e) A three-dimensional plot of the frequency of the J_{SC} depending on variable vertical displacements and rotation speeds. Reproduced with permission from American Chemical Society [34].

self-powered displacement sensor, which can also be visualized through direct powering of LEDs. The self-powered displacement sensor could have unique applications like monitoring the thickness of the braking pad in automobiles. On the other hand, the J_{SC} under a series of rotation speeds ranging from 100 rpm to 1000 rpm was measured with a constant vertical distance at d=0.5 mm, and it could be clearly found that the J_{SC} increased linearly with the rotation speed, since the output current was the time differentiation of the transferred charges across the external load. In the meanwhile, it is also shown in the figure that the frequency of the J_{SC} also exhibits perfect linear relationship to the rotation speed. Therefore, the FRD-TENG could be employed as a self-powered rotation speed sensor by analyzing both the magnitude and frequency of the measured J_{SC}. Thus, the rotation speed and the vertical separation distance were two input parameters influencing the output current signal, which could be characterized by the magnitude and the frequency. In order to illustrate this two-fold relationship and show a comprehensive working characteristic of the FRD-TENG as a self-powered sensor, two sets of experiments were carried out to give three-dimensional plots of the two-fold dependence of the magnitude (Fig. 10d) and frequency (Fig. 10e) on the vertical displacement and the rotation speed, respectively. As expected, the magnitude was affected by both the vertical displacement and the rotation speed, while the frequency was only affected by the rotation speed. From these results, the information about two important parameters of a mechanical motion could be solely determined by the measured profiles of the J_{SC}. Based on this principle, the FRD-TENG could be employed as a self-powered mechanical sensor in automobiles to detect both the radial and axial movement of a braking pad at the same time. This two-parameter monitoring approach provided us deeper insights on the application of nanogenerator in self-powered system and exhibited unique advantages than the existing single-parameter active sensors.

Through combing the structures of cylindrical TENGs that can serve as self-power rotation sensor [45] and case-encapsulated TENGs that can serve self-powered linear sliding sensors [62], a TENG-based dual-mode, self-powered

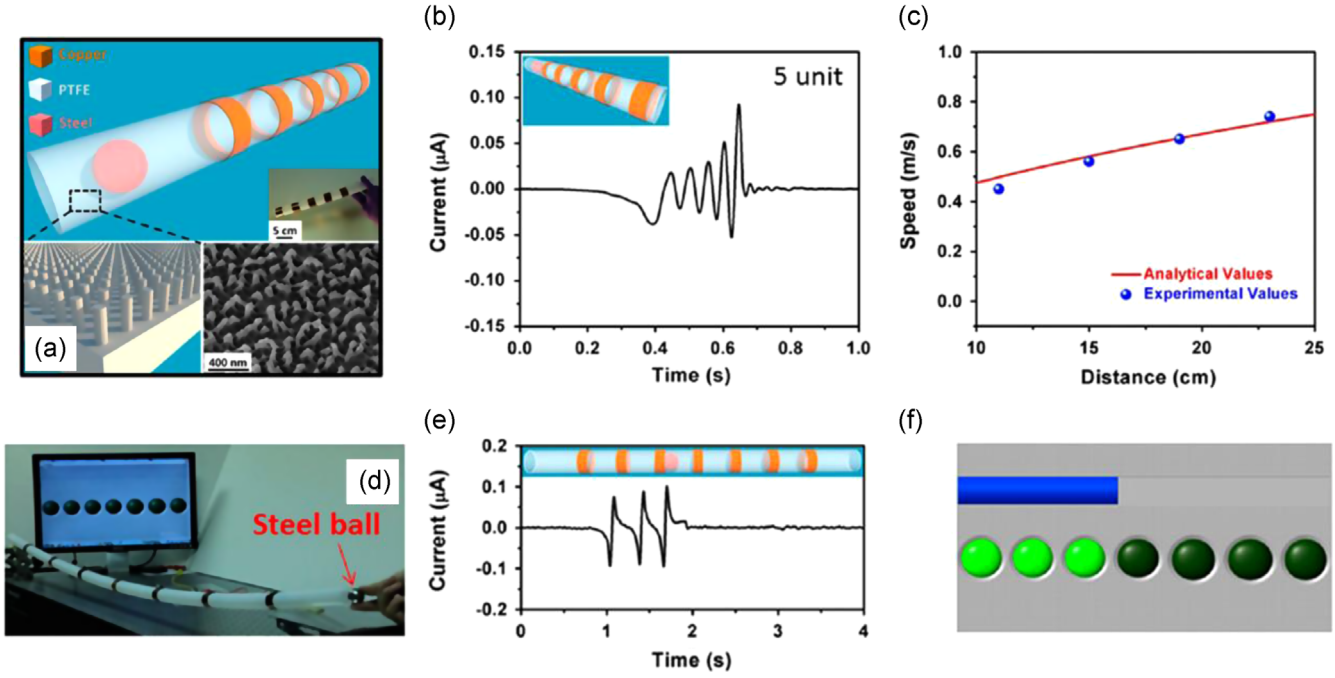

Fig. 11 Triboelectric sensor for self-powered tracking of object motion inside a tube. (a) The schematic structure of the tube-shaped triboelectric sensor that could track the motion of an object inside the tube. (b) The measurement of the output current of the single-electrode triboelectric sensor with five grating electrodes. (c) The calculated motion speed of the steel ball with variable distances from both experimental and analytical results. (d) A photograph showing the real time measurement of the motion tracking of the steel ball inside tubing. (e) The measurement result of the output current when the steel ball passed the first three grating electrodes. (f) The real time location visualization of the ball motion inside tubing. Reproduced with permission from American Chemical Society [64].

velocity sensor for rectified linear and rotary motions has been reported [63]. Employing alternating Kapton-copper strips arranged in a spiral configuration on the inner and outer surfaces of two concentric cylinders, voltage assays for linear and rotary motions can be measured without applying an external power source. The triboelectric generated output signals when integrated with a digital circuit and a microcontroller unit (MCU) can be directly processed into velocity information. Linear speeds of 0.1–0.6 m/s and rotary speeds of 125–700 rpm have been measured with high stability.

TENGs for self-powered tracking of a moving object

By simply integrating multiple single-electrode triboelectric sensors into an array device, the self-powered motion tracking of an arbitrary moving object could be obtained with the information like the location, speed, and acceleration of the object. In this regard, the prototype of the first single-electrode TENG matrix has been developed for self-powered tracking of the touching behavior and applied pressure [26].

Then, a series of single-electrode triboelectric sensors (SE-TES) [64] was integrated into a one-dimensional array of tube structures consisting of tube-shaped PTFE thin film and grating copper electrodes for tracking the motion status (location, speed) of a steel ball moving inside the tubing, as shown in Fig. 11a. As the steel ball rolled across a Cu electrode, pulsed outputs of the open-circuit voltage and short-circuit current measured between the electrode and the ground reach 60 V and 0.4 μA, respectively. In order to track the traveling velocity of the steel ball inside the PTFE tube, five Cu electrodes were evenly distributed along the PTFE tube with a uniform interval and were connected in parallel to a positive probe of an electrometer. With the PTFE tube having a tilt angle of 15° to the horizontal plane, the measured currents from devices having five grating electrodes were shown in Fig. 11b. The analysis in Fig. 11c provided two-fold information of the ball motion. First, the position of the ball could be identified based on the correspondence with the pulsed current signals; second, the average moving speed could be determined by the time interval between two consecutive current peaks. It could be found that the results from both analytic values and experimental data reached good agreement, indicating the validity of this measurement approach. The sensitivity and reliability of the SE-TES were further evaluated with variable tilting angles. Moreover, to demonstrate the practical application of the SE-TES in motion tracking, the device was developed into a seven-electrode structure for real time mapping of the ball location inside tubing, along with LED indicators from Labview software, as shown in Fig. 11d. From the real time current measurement result (Fig. 11e) and the turning on of LED indicators, it could be confirmed that this self-powered motion tracking system could clearly identify the motion of the steel balls inside tubing. This work had demonstrated the potential application of the SE-TES in pipeline blockage inspection.

Besides this work, a two-dimensional array of the SE-TES was developed to actively detect the position, displacement,

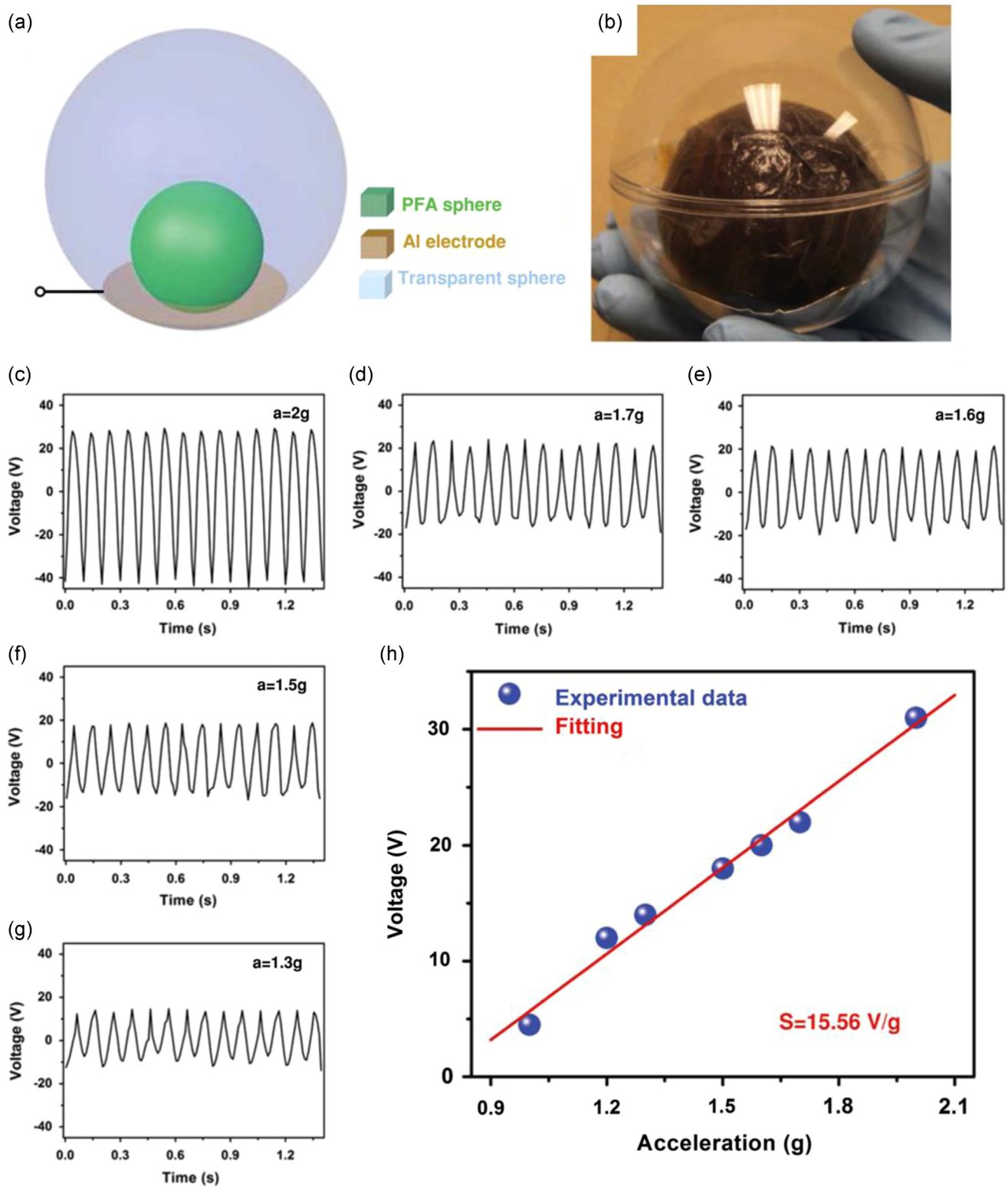

Fig. 12 Triboelectric nanogenerator as a self-powered acceleration sensor. (a) The schematic diagram showing the device structure of a spherical TENG. (b) Photograph of a fabricated TENG. (c-g) Output voltage of the sensor subjected with certain acceleration. (h) Dependence of the output voltage on the acceleration. Reproduced with permission from Wiley [69].

velocity, and acceleration of the moving object through measuring open-circuit voltage and short-circuit current in real time [65]. The detected velocity and acceleration of the moving object has an average error of ~0.265% and ~2.5%, respectively. The velocity could also be detected by utilizing the amplitude of the short-circuit current, which had a sensitivity of ~887 pA/(cm s^{-1}). Additionally, LED illuminations were connected to each sensor unit and used as real-time indicators to monitor the motion of a sliding object and walking steps of a human. This triboelectric motion sensor

has ubiquitous applications in various fields such as automation, robotics, and safety control.

Through designing a cross-bar grid electrode structure, a self-powered velocity and trajectory tracking sensor (VTTS) array for detecting object motion, velocity, acceleration and trajectory has been developed, which is enabled by single-electrode TENGs [66]. A self-powered VTTS arrays (9×9 pixel) with low-node mode has realized the real-time tracking of position, velocity, acceleration and trajectory for a moving object by visual observation. Using the simply electrode weave technique, a high-resolution VTTS with 41×41 pixel on an active size of 1×1 cm^2 was obtained and it only needs 82 output ports. The device can detect a tiny displacement and trajectory for the high resolution of 250 μm.

TENG as self-powered acceleration sensors

Acceleration is one of the most important parameters in the characterization of an object's movement. Usually, the acceleration sensors are based on force sensing mechanisms, including piezoresistive or differential capacitance, which has a wide variety of applications for industrial engineering, biology and navigation [67,68]. An external power source is indispensable to drive these sensors. For realizing the self-powered operation, a newly designed 3D-TENG has been developed as an active acceleration sensor [69]. The spherical TENG consists of two spheres, as shown in Fig. 12a. An ordinary rubber ball was coated with etched PFA film to form a PFA ball, where the PFA film acts as a triboelectric polymer. The inner PFA ball can slide and bounce freely inside the transparent shell. A thin Al foil was adhered to the inner surface of the outer sphere, acting as both the triboelectric layer and the electrode. Fig. 12b displays a corresponding photograph of TENG. In order to enhance the performance of the TENG, the PFA film was dry-etched using ICP to create the nanoparticle-like structures on the surface. The fabricated TENG can scavenge the vibration energy in full space by working at a hybridization of both the contact-separation mode and the sliding mode.

When the spherical TENG serves as a self-powered acceleration sensor, the output voltages of the sensor at specific acceleration are enumerated in Fig. 12c–g. It can be seen clearly that all of the output voltage signals are uniform and stable. The relationship between output voltage and acceleration is plotted in Fig. 12h, revealing a clear linear relationship by fitting the data, which is beneficial for practical applications of the sensors. The detection sensitivity of the acceleration was calculated to be about 15.56 V/g.

Triboelectric nanogenerators as self-powered active chemical/environmental sensors

Through using the environmental factors to alter the properties of one of the triboelectric layers in a TENG, it has been developed as the self-powered active sensor for the changes in the environment, e.g. the concentration of certain chemical species [37,38,70,71], the UV illumination [72].

TENGs as self-powered active chemical sensors

In the basic working principles of TENGs, the amplitudes of the generated electrical signals (V_{OC} and I_{SC}) are all proportional to the triboelectric charge density when all the other conditions are maintained same. Since the driving force for the triboelectrification process is basically the chemical potential difference between the two surfaces, the absorption of certain chemical species or molecules on the surface could influence the triboelectric charge density, thus the electrical output from the TENG. In this way, through purposely modifying one of the triboelectric surfaces to enable an effective absorption to the targeted species/molecules, the TENG has been developed as the self-powered active chemical sensors.

In the year of 2013, our group has shown that the principle of the TENG can be used as a sensor for the detection of Hg^{2+} ions [37]. The first step is to assemble Au nanoparticles (NPs) onto the metal plate, which can help to improve the performance of the TENG. These assembled Au NPs could enlarge the contact area of the two plates, which will increase the electrical output of the TENG. Through further modifying the assembled Au NPs with 3-mercaptopropionic acid (3-MPA) molecules, the high-output nanogenerator can serve as a highly sensitive and selective nanosensor for Hg^{2+} ions detection based on the different triboelectric polarities of Au NPs and Hg^{2+} ions. The TENG has a layered structure based on two plates (Fig. 13a). Glass was selected as the substrate owing to its strength, light weight, and low cost. On the lower side, the metal plate is prepared. The metal plate consists of an Au thin film and assembled Au NPs, which plays dual roles of electrode and contact material. Through utilizing 1,3-propanedithiol as the linker molecules, Au NPs of different sizes were uniformly assembled onto the surface of Au film (Fig. 13b–d). Au NPs were prepared by the reduction of Au^{3+} ions with sodium citrate, which also acted as a capping agent to stabilize the as-prepared Au NPs. For the purpose of selective detection of Hg^{2+} ions, 3-MPA was self-assembled onto the surface of Au NPs through strong Au-S interactions. Its recognition of Hg^{2+} ions enables Hg^{2+} ions to selectively bind to the Au NP surface. On the other plate, another Au thin film is laminated between the glass substrate and a layer of PDMS. Here, PDMS and Au are extremely different in their abilities to attract and retain electrons in the triboelectric series. Such a TENG was demonstrated as a self-powered device for detecting molecular species. Fig. 13e shows the output of the pristine TENG by using a full-wave rectifying bridge. For the selective detection of Hg^{2+} ions, the Au plate was then soaked with the Tris-borate (50 mM, pH9) buffer solution containing various concentrations of Hg^{2+} ions and other metal ions at ambient temperature. After the interaction with Hg^{2+} ions (5 mM), the generated J_{SC} of TENG decreased from 63 mA/cm^2 to 8 mA/cm^2 (Fig. 13f). This is because that the adsorbed molecular species modify the triboelectric behavior, which enables the detection of the Hg^{2+} concentration. By observing TENG performance with an LED bulb, we could build a fully standalone and self-powered environmental sensing device, which demonstrates the TENG's capability of being an environmental sensor without any supporting equipment (power source, capacitor, and electrometer). Fig. 13g shows that the electrical signal of the TENG decreased upon increasing the

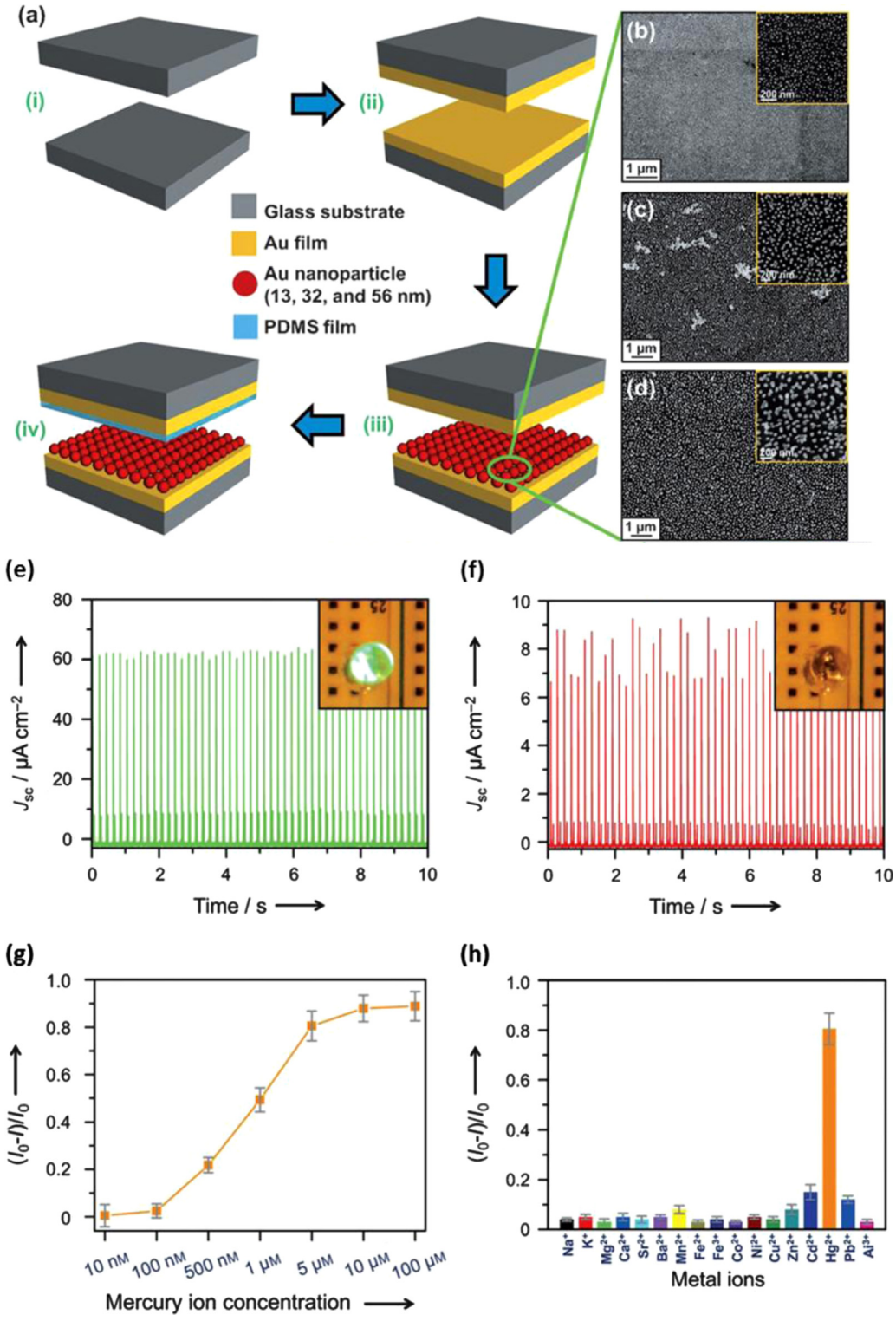

Fig. 13 An TENG as a self-powered active nanosensor for mercury ion detection. (a) Fabrication process of the triboelectric nanogenerator (TENG). (b)-(d) SEM images of the Au film modified with (b) 13 nm, (c) 32 nm, and (d) 56 nm Au NPs. Scale bars: (b)-(d) 1 mm; insets: 200 nm. (e) and (f) Rectified J_{SC} of the as-developed TENG before (e) and after (f) the interaction with 5 mM Hg^{2+} ions. Insets: photograph of the indicated LED lamp before (e) and after (f) interaction with 5 mM Hg^{2+} ions, as an indication of detected concentration. (g) Sensitivity and (h) selectivity of the as-developed TENG for the detection of Hg^{2+} ions. The concentration of all metal ions tested in the selectivity experiment was 5 mM. Reproduced with permission from Wiley [37].

concentration of Hg^{2+} ions, with a linear relationship between the short-circuit current ratio $((I_0-I)/I_0)$ and the concentration of Hg^{2+} ions ranging from 100 nm to 5 mm ($R^2=0.98$). This approach provides a detection limit at an S/N of 3 at 30 nM for Hg^{2+} ions. Control experiments were carried out to test the selectivity of the developed system toward Hg^{2+} ion detection as compared to other metal ions (each at a concentration of 5 mM). The results displayed in Fig. 13h reveal that the sensing system is specific to Hg^{2+} ions, which comes from the high selectivity of 3-MPA toward Hg^{2+} ions resulted from the carboxylic acid. The potential interference metal ions could not bind to 3-MPA-modified Au NPs, resulting in negligible changes in the electrical signal of the TENG.

Following the above-described work, our group has developed the triboelectric effect-based nanosensor for catechin detection by utilizing TiO_2 nanomaterial array as the probe and contact material [38]. This novel self-powered TENG is highly sensitive (detection limit of 5 μM and linear range of 10 μM to 0.5 mM) and selective for catechin detection, demonstrating great potential for the determination of catechin concentrations in real samples. The output voltage and current density of the as-developed TENG can be enhanced from 4.3 V to 21.3 V and 1.1 μA/cm^2 to 3.2 μA/cm^2, respectively, when detecting catechin concentration over 0.5 mM.

Through utilizing the contact-electrification between water (as well as other liquids) and insulating polymers, water-based TENGs have been developed, which can serve as self-powered chemical and temperature sensors for the liquid [73]. For example, it has been experimentally demonstrated that the increase of the ethanol concentration in water-based solution will result in the decrease of the TENG's electrical output. It should come from the mixing with ethanol decreasing the water polarity, which could enhance the interaction with hydrophobic PDMS film, and consequently reducing the triboelectric charge density and generated output by the TENG. Temperature has been studied as other key factor to affect the dielectric constant and polarity of water. A similar tendency between water temperature and generated output was observed. These two sets of results indicate that the water–TENG can be applied to detect substances that will change the dielectric constant and/or polarity of water.

TENGs as self-powered active UV sensors

UV photodetectors have been widely used in communications, biological and chemical analysis, environmental monitoring, remote control, memory storage, and optoelectronic circuits. Some prototype self-powered UV sensor based on photoelectrochemical cell and p-n junction have been reported. Through fully integrating photodetector for UV light sensing with the TENG conformation, a self-powered active UV sensor was developed [72]. 3D dendritic TiO_2 nanostructures serve not only as the built-in photodetector but also as one of the triboelectric layers in the TENG. The fabrication process of the active UV photodetector is shown in Fig. 14a. The demonstrated device is constituted by a layered structure of two plates. On the lower side, the TiO_2 plate is prepared. First, 3D dendritic TiO_2 nanostructures were growth on a glass substrate through the chemical bath deposition method. Then a colorless thin film of ITO was deposited on the back of the 3D dendritic TiO_2 nanostructures coated glass substrate as the conducting electrode. On the other plate, another ITO thin film was deposited between a glass substrate and a PDMS. Finally, the Ni thin film was selected to deposit as the electrodes of the built-in photodetector to achieve the Schottky contact. The built-in photodetector is then connected with the TENG to construct the active UV sensor. The resistance of the built-in photodetector varies upon UV light irradiation with different intensities, which will consequently influence the measured output of the TENG from the two leads. In this way, the light intensity can be determined by monitoring the output of the TENG.

As serially connecting the build-in photodetector to TENG, a new type of self-powered UV sensor was demonstrated, in which the photodetector acts as the external load for the TENG. Since the TENG's output obtained by the load has a direct dependence to the load resistance, the change of the build-in photodetector's resistance will lead to the change of the measured output amplitudes. In the dark, the resistance of built-in photodetector is larger, hence the output current will be lower and the output voltage will be higher and closed to the open circuit voltage (V_{OC}). Under UV light irradiation, the resistance of built-in photodetector decreases. The output current of the self-powered photodetector when sensing UV light at different intensity is displayed in Fig. 14b. The output current increases from 2 nA (in the dark) to 0.7 μA when the power intensity of incident UV light is varied to 7 mW/cm^2. The dependence of the output current on the incident light power density can be seen more clearly from Fig. 14c. It is found that the output current has a linear relationship with the incident light power density from 20 μW/cm^2 to 7 mW/cm^2. On the other hand, the output voltage diminishes to 4.8 V when the power intensity of incident UV light is increased to 7 mW/cm^2. Although a linear relationship between the output voltage and incident light power intensity is also observed (Fig. 14d), the change of the output current from the intensity of the incident UV light can reach up to 2 orders of magnitude, which is thus more convenient for the determination of the UV light intensity. The responsivity of the active UV photodetectoris displayed in Fig. 14e. This active UV photodetector exhibits an excellent capability of detecting the incident light with the intensity ranging from 20 μW/cm^2 to 7 mW/cm^2, which is more sensitive than the self-powered UV photodetector based on p-n junction.

Summary and perspectives

In the recent decades, electronic devices and systems are becoming more and more personal, portable, complex, multi-functional and smart. They are taking increasingly important roles in people's daily life. In all of the electronic devices/systems with different functionalities, sensors are the keys not only for such devices and systems to interact with people and environment, but also for different components to work coordinately with each other. In order to enable the system to work wirelessly, sustainably and independently, it is highly desirable to enable the self-powered

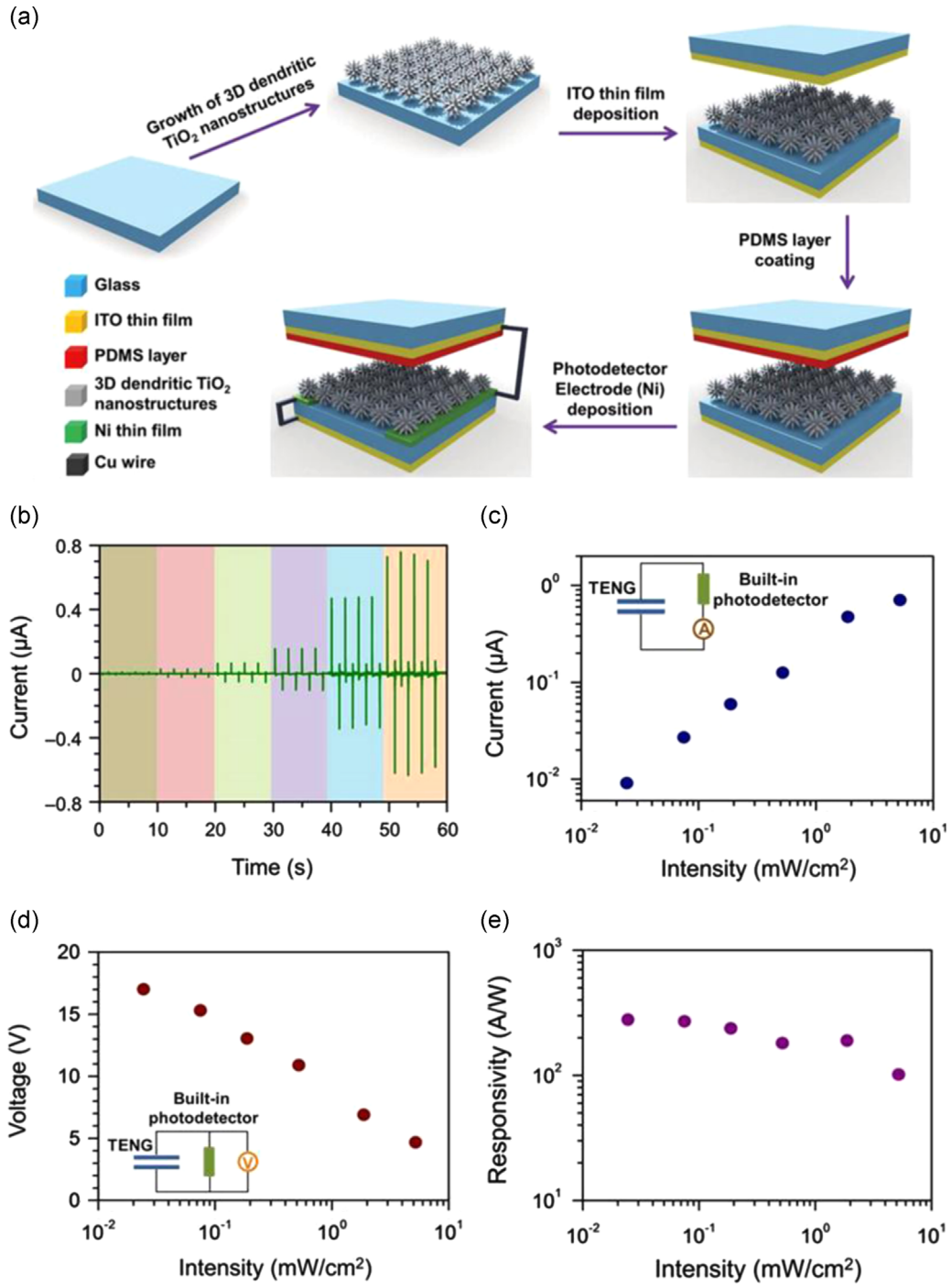

Fig. 14 An TENG as a self-powered active UV sensor. (a) Fabrication process of the self-powered UV photodetector. (b) Output current of the self-powered sensor under UV light illumination with various power intensities. (c–e) The dependence of output current (c), output voltage (d), and responsivity (e) of the self-powered UV sensor on the light intensities. Reproduced with permission from Wiley [72].

operation on the sensors, which means that their operations do not rely on external power source. With the huge advantages of extremely high output and efficiency, low fabrication cost, outstanding stability/robustness and environmental friendly, the invention of triboelectric nanogenerators in the year of 2012 is not only a disruptive technology in the field of mechanical energy harvesting, but also provides a new category of sensors—self-powered active sensors that can directly generate electrical signal as a response to applied mechanical stimuli. The information of mechanical stimuli and environmental conditions is directly reflected by the self-generated electrical signals, which does not require an external power source. Since the TENGs can effectively utilize mechanical energies in almost any form and any scale under the four fundamental modes, they can serve as the self-powered mechanical sensors for a wide range of different mechanical agitations, such as pressure, touching, vibration, linear fine displacement, rotation, tracking of moving objects,

acceleration. Moreover, the TENGs can also be applied as self-powered active chemical sensors based on the proportional relationship between the amplitudes of the electrical signals generated by TENGs and the surface triboelectric charge density that is mostly determined by surface chemical state. The application of self-powered active sensors reduces the power consumption of the entire system, decreases the complexity of the system, and more importantly enables the sustainable, independent and maintenance-free operation. This new type of self-powered active sensor is bringing the sensor technology into a new paradigm.

In the future, the continuous efforts on TENGs as self-powered active sensors will largely improve their performance and real applicability in wireless sensor networks, through the researches in the following direction. The deepened understanding of triboelectrification and the surface modification/functionalization will help to achieve a higher triboelectric charge density, which will further enhance the sensitivity of the TENG-based sensors. Through adopting innovative device structural designs, the application of the TENG-based self-powered sensors can be largely broadened for sensing different mechanical behaviors from a variety of different sources. Moreover, the integration with other modules in sensor systems (e.g. signal detection and post-processing components) and the realization of self-powered operation for entire wireless sensor nodes including the supporting components (e.g. wireless transmitter for the signals) will eventually enable the true application of TENGs as active self-powered sensors in wireless sensor networks. It can be anticipated that through the worldwide efforts on TENGs as self-powered active sensors they will soon become commercially available to have broad impact in medical sciences, infrastructure/environmental monitoring, defense technology, and even personal electronics.

Acknowledgements

Research was supported by BES DOE (DE-FG02-07ER46394), NSF, Airforce, Samsung, SKKU (Korea), MANA NIMS (Japan), and the Knowledge Innovation Program of the Chinese Academy of Sciences (KJCX2-YW-M13), the Hightower Chair Foundation, and the “thousands talents” program for pioneer researcher and his innovation team, China. We thank Fengru Fan, Guang Zhu, Ya Yang, Zong-Hong Lin, Youfan Hu, Jin Yang, Yusheng Zhou, Jun Chen, Yuanjie Su, Hulin Zhang, Weiqing Yang, Yannan Xie, Simiao Niu, Gang Cheng, Peng Bai, Xiaonan Wen, Caofeng Pan, Qingshen Jing, Fang Yi, Ying Liu, Liming Zhang, Chang Bao Han and Chi Zhang for their contributions to the works reviewed here.

References

[1] J. Yick, B. Mukherjee, D. Ghosal, Comput. Netw. 52 (2008) 2292–2330.
[2] Z.L. Wang, Sci. Am. 298 (2008) 82.
[3] Z.L. Wang, Adv. Mater. 24 (2012) 280–285.
[4] Z.L. Wang, W.Z. Wu, Angew. Chem. Int. Ed. 51 (2012) 11700–11721.
[5] Z.L. Wang, J.H. Song, Science 312 (2006) 242–246.
[6] Z.L. Wang, G. Zhu, Y. Yang, S.H. Wang, C.F. Pan, Mater. Today 15 (2012) 532–543.
[7] S. Xu, B.J. Hansen, Z.L. Wang, Nat. Commun. 1 (2010) 93. http://dx.doi.org/10.1038/ncomms1098.
[8] R.S. Yang, Y. Qin, L.M. Dai, Z.L. Wang, Nat. Nanotechnol. 4 (2009) 34–39.
[9] Y. Qin, X.D. Wang, Z.L. Wang, Nature 451 (2008) 809–813.
[10] X.D. Wang, J.H. Song, J. Liu, Z.L. Wang, Science 316 (2007) 102–105.
[11] G.S.P. Castle, J. Electrostat. 40-1 (1997) 13–20.
[12] A.F. Diaz, R.M. Felix-Navarro, J. Electrostat. 62 (2004) 277–290.
[13] L.S. McCarty, G.M. Whitesides, Angew. Chem. Int. Ed. 47 (2008) 2188–2207.
[14] H.T. Baytekin, A.Z. Patashinski, M. Branicki, B. Baytekin, S. Soh, B.A. Grzybowski, Science 333 (2011) 308–312.
[15] Z.L. Wang, ACS Nano 7 (2013) 9533–9557.
[16] F.R. Fan, Z.Q. Tian, Z.L. Wang, Nano Energy 1 (2012) 328–334.
[17] F.R. Fan, L. Lin, G. Zhu, W.Z. Wu, R. Zhang, Z.L. Wang, Nano Lett. 12 (2012) 3109–3114.
[18] G. Zhu, C.F. Pan, W.X. Guo, C.Y. Chen, Y.S. Zhou, R.M. Yu, Z.L. Wang, Nano Lett. 12 (2012) 4960–4965.
[19] S.H. Wang, L. Lin, Z.L. Wang, Nano Lett. 12 (2012) 6339–6346.
[20] G. Zhu, J. Chen, Y. Liu, P. Bai, Y.S. Zhou, Q.S. Jing, C.F. Pan, Z.L. Wang, Nano Lett. 13 (2013) 2282–2289.
[21] L. Lin, S.H. Wang, Y.N. Xie, Q.S. Jing, S.M. Niu, Y.F. Hu, Z.L. Wang, Nano Lett. 13 (2013) 2916–2923.
[22] S.H. Wang, Y.N. Xie, S.M. Niu, L. Lin, Z.L. Wang, Adv. Mater. 26 (2014) 2818–2824.
[23] G. Zhu, J. Chen, T.J. Zhang, Q.S. Jing, Z.L. Wang, Nat. Commun. 5 (2014) 3426.
[24] S.H. Wang, Z.H. Lin, S.M. Niu, L. Lin, Y.N. Xie, K.C. Pradel, Z.L. Wang, ACS Nano 7 (2013) 11263–11271.
[25] B. Meng, W. Tang, Z.H. Too, X.S. Zhang, M.D. Han, W. Liu, H.X. Zhang, Energy Environ. Sci 6 (2013) 3235–3240.
[26] Y. Yang, Y.S. Zhou, H.L. Zhang, Y. Liu, S.M. Lee, Z.L. Wang, Adv. Mater. 25 (2013) 6594–6601.
[27] S.H. Wang, Y.N. Xie, S.M. Niu, L. Lin, C. Liu, Y.S. Zhou, Z.L. Wang, Adv. Mater. 26 (2014) 6720–6728.
[28] G. Zhu, W.Q. Yang, T.J. Zhang, Q.S. Jing, J. Chen, Y.S. Zhou, P. Bai, Z.L. Wang, Nano Lett. 14 (2014) 3208–3213.
[29] Y. Yang, H.L. Zhang, Z.H. Lin, Y.S. Zhou, Q.S. Jing, Y.J. Su, J. Yang, J. Chen, C.G. Hu, Z.L. Wang, ACS Nano 7 (2013) 9213–9222.
[30] L. Lin, Y.N. Xie, S.H. Wang, W.Z. Wu, S.M. Niu, X.N. Wen, Z.L. Wang, ACS Nano 7 (2013) 8266–8274.
[31] G. Zhu, Z.-H. Lin, Q.S. Jing, P. Bai, C.F. Pan, Y. Yang, Y.S. Zhou, Z.L. Wang, Nano Lett. 13 (2013) 847–853.
[32] S.H. Wang, L. Lin, Y.N. Xie, Q.S. Jing, S.M. Niu, Z.L. Wang, Nano Lett. 13 (2013) 2226–2233.
[33] G. Zhu, Y.S. Zhou, P. Bai, X.S. Meng, Q.S. Jing, J. Chen, Z.L. Wang, Adv. Mater. 26 (2014) 3788–3796.
[34] L. Lin, S.H. Wang, S.M. Niu, C. Liu, Y.N. Xie, Z.L. Wang, ACS Appl. Mater. Interfaces 6 (2014) 3038–3045.
[35] J. Chen, G. Zhu, W.Q. Yang, Q.S. Jing, P. Bai, Y. Yang, T.C. Hou, Z.L. Wang, Adv. Mater. 25 (2013) 6094–6099.
[36] J. Yang, J. Chen, Y. Liu, W.Q. Yang, Y.J. Su, Z.L. Wang, ACS Nano 8 (2014) 2649–2657.
[37] Z.H. Lin, G. Zhu, Y.S. Zhou, Y. Yang, P. Bai, J. Chen, Z.L. Wang, Angew. Chem. Int. Ed. 52 (2013) 5065–5069.
[38] Z.H. Lin, Y.N. Xie, Y. Yang, S.H. Wang, G. Zhu, Z.L. Wang, ACS Nano 7 (2013) 4554–4560.
[39] J.A. Wiles, B.A. Grzybowski, A. Winkleman, G.M. Whitesides, Anal. Chem. 75 (2003) 4859–4867.
[40] Z.L. Wang, Faraday Discuss. (2014). http://dx.doi.org/10.1039/C4FD00159A.
[41] Y.F. Hu, J. Yang, Q.S. Jing, S.M. Niu, W.Z. Wu, Z.L. Wang, ACS Nano 7 (2013) 10424–10432.
[42] J. Yang, J. Chen, Y. Yang, H.L. Zhang, W.Q. Yang, P. Bai, Y.J. Su, Z.L. Wang, Adv. Energy Mater 4 (2014) 1301322.
[43] W.Q. Yang, J. Chen, G. Zhu, J. Yang, P. Bai, Y.J. Su, Q.S. Jing, X. Cao, Z.L. Wang, ACS Nano 7 (2013) 11317–11324.

[44] X.N. Wen, W.Q. Yang, Q.S. Jing, Z.L. Wang, ACS Nano 8 (2014) 7405–7412.
[45] P. Bai, G. Zhu, Y. Liu, J. Chen, Q.S. Jing, W.Q. Yang, J.S. Ma, G. Zhang, Z.L. Wang, ACS Nano 7 (2013) 6361–6366.
[46] Y. Yang, H.L. Zhang, J. Chen, Q.S. Jing, Y.S. Zhou, X.N. Wen, Z.L. Wang, ACS Nano 7 (2013) 7342–7351.
[47] S.M. Niu, Y. Liu, S.H. Wang, L. Lin, Y.S. Zhou, Y.F. Hu, Z.L. Wang, Adv. Funct. Mater. 24 (2013) 3332–3340.
[48] H.L. Zhang, Y. Yang, X.D. Zhong, Y.J. Su, Y.S. Zhou, C.G. Hu, Z.L. Wang, ACS Nano 8 (2014) 680–689.
[49] Y.N. Xie, S.H. Wang, S.M. Niu, L. Lin, Q.S. Jing, J. Yang, Z.Y. Wu, Z.L. Wang, Adv. Mater. 26 (2014) 6599–6607.
[50] S.H. Wang, S.M. Niu, J. Yang, L. Lin, Z.L. Wang, ACS Nano (2014). http://dx.doi.org/10.1021/nn5054365.
[51] Y. Yang, H.L. Zhang, X.D. Zhong, F. Yi, R.M. Yu, Y. Zhang, Z.L. Wang, ACS Appl. Mater. Interfaces 6 (2014) 3680–3688.
[52] Y. Yang, L. Lin, Y. Zhang, Q.S. Jing, T.C. Hou, Z.L. Wang, ACS Nano 6 (2012) 10378–10383.
[53] P. Bai, G. Zhu, Q.S. Jing, J. Yang, J. Chen, Y.J. Su, J.S. Ma, G. Zhang, Z.L. Wang, Adv. Funct. Mater. 24 (2014) 5807–5813.
[54] W.Q. Yang, J. Chen, X.N. Wen, Q.S. Jing, J. Yang, G. Zhu, W. Z. Wu, Z.L. Wang, ACS Appl. Mater. Interfaces 6 (2014) 7479–7484.
[55] L.M. Zhang, F. Xue, W.M. Du, C.B. Han, C. Zhang, Z.L. Wang, Nano Res 7 (2014) 1215–1223.
[56] J. Bernstein, R. Miller, W. Kelley, P. Ward, J. Microelectromech. Syst. 8 (1999) 433–438.
[57] Y. Itakura, N. Fujii, T. Sawada, Phys. Chem. Earth Part B 25 (2000) 717–720.
[58] A.F. Yu, P. Jiang, Z.L. Wang, Nano Energy 1 (2012) 418–423.
[59] W.Q. Yang, J. Chen, Q.S. Jing, J. Yang, X.N. Wen, Y.J. Su, G. Zhu, P. Bai, Z.L. Wang, Adv. Funct. Mater. 24 (2014) 4090–4096.
[60] W.Q. Yang, J. Chen, G. Zhu, X.N. Wen, P. Bai, Y.J. Su, Y. Lin, Z.L. Wang, Nano Res 6 (2013) 880–886.
[61] Y.S. Zhou, G. Zhu, S.M. Niu, Y. Liu, P.S. Bai, Q. Jing, Z.L. Wang, Adv. Mater. 26 (2014) 1719–1724.
[62] Q.S. Jing, G. Zhu, P. Bai, Y.N. Xie, J. Chen, R.P.S. Han, Z.L. Wang, ACS Nano 8 (2014) 3836–3842.
[63] Q.S. Jing, G. Zhu, W.Z. Wu, P. Bai, Y.N. Xie, J. Chen, R.P. S. Han, Z.L. Wang, Nano Energy 10 (2014) 305–312.
[64] Y.J. Su, G. Zhu, W.Q. Yang, J. Yang, J. Chen, Q.S. Jing, Z.M. Wu, Y.D. Jiang, Z.L. Wang, ACS Nano 8 (2014) 3843–3850.
[65] F. Yi, L. Lin, S.M. Niu, J. Yang, W.Z. Wu, S.H. Wang, Q.L. Liao, Y. Zhang, Z.L. Wang, Adv. Funct. Mater. (2014). http://dx.doi.org/10.1002/adfm.201402703.
[66] C.B. Han, C. Zhang, X.H. Li, L.M. Zhang, T. Zhou, W.G. Hu, Z.L. Wang, Nano Energy 9 (2014) 325–333.
[67] A. Kazama, T. Aono, R. Okada, J. Microelectromech. Syst. 22 (2013) 386–394.
[68] R. Kuells, S. Nau, M. Salk, K. Thoma, Sensor Actuat. A-Phys. 182 (2012) 41–48.
[69] H.L. Zhang, Y. Yang, Y.J. Su, J. Chen, K. Adams, S. Lee, C.G. Hu, Z.L. Wang, Adv. Funct. Mater. 24 (2014) 1401–1407.
[70] H.L. Zhang, Y. Yang, Y.J. Su, J. Chen, C.G. Hu, Z.K. Wu, Y. Liu, C.P. Wong, Y. Bando, Z.L. Wang, Nano Energy 2 (2013) 693–701.
[71] Z.H. Lin, G. Cheng, W.Z. Wu, K.C. Pradel, Z.L. Wang, ACS Nano 8 (2014) 6440–6448.
[72] Z.H. Lin, G. Cheng, Y. Yang, Y.S. Zhou, S. Lee, Z.L. Wang, Adv. Funct. Mater. 24 (2014) 2810–2816.
[73] Z.H. Lin, G. Cheng, L. Lin, S. Lee, Z.L. Wang, Angew. Chem. Int. Ed. 52 (2013) 12545–12549.

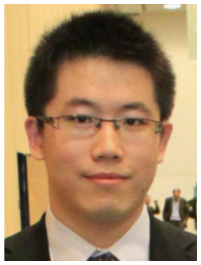

Sihong Wang is currently a postdoctoral fellow in Prof. Zhong Lin (Z.L.) Wang's group at the Georgia Institute of Technology. He obtained his Ph.D. degree in Materials Science and Engineering from the Georgia Institute of Technology in 2014 under the supervision of Prof. Zhong Lin (Z.L.) Wang, and his B.S. in Materials Science and Engineering from Tsinghua University, China in 2009. His research mainly focuses on nanomaterial-based mechanical energy harvesting and energy storage, self-powered systems, nanogenerator-based sensors and piezotronics.

Long Lin received his B.S. in Materials Science and Engineering from Tsinghua University, China in 2010. He is currently a Ph. D. candidate in School of Materials Science and Engineering at Georgia Institute of Technology. He is working as a graduate research assistant in Prof. Zhong Lin Wang's group. His research interests include developing high-output piezoelectric nanogenerator based on rational assembly of semiconductor nanowires, establishing the concept and various prototypes of triboelectric nanogenerators for mechanical energy harvesting, developing self-powered systems and active sensors for the practical applications of nanogenerators.

Zhong Lin Wang received his Ph.D. from Arizona State University in physics. He now is the Hightower Chair in Materials Science and Engineering, Regents' Professor, Engineering Distinguished Professor and Director, Center for Nanostructure Characterization, at Georgia Tech. Dr. Wang has made original and innovative contributions to the synthesis, discovery, characterization and understanding of fundamental physical properties of oxide nanobelts and nanowires, as well as applications of nanowires in energy sciences, electronics, optoelectronics and biological science. His discovery and breakthroughs in developing nanogenerators established the principle and technological road map for harvesting mechanical energy from environment and biological systems for powering a personal electronics. His research on self-powered nanosystems has inspired the worldwide effort in academia and industry for studying energy for micro-nano-systems, which is now a distinct disciplinary in energy research and future sensor networks. He coined and pioneered the field of piezotronics and piezo-phototronics by introducing piezoelectric potential gated charge transport process in fabricating new electronic and optoelectronic devices. Details can be found at: www.nanoscience.gatech.edu.